Structural Engineering and Mechanics, *Vol. 74, No. 1 (2020) 33-54*
DOI: https://doi.org/10.12989/sem.2020.74.1.033

Free vibration and harmonic response of cracked frames using a single variable shear deformation theory

Baran Bozyigit[1a] and Yusuf Yesilce[1b] and Magd Abdel Wahab[2,3] *

[1]*Department of Civil Engineering, Dokuz Eylul University, Buca, Izmir, Turkey*
[2]*Division of Computational Mechanics, Ton Duc Thang University, Ho Chi Minh City, Vietnam*
[3]*Faculty of Civil Engineering, Ton Duc Thang University, Ho Chi Minh City, Vietnam*

(Received April 3, 2019, Revised August 28, 2019, Accepted November 12, 2019)

Abstract. The aim of this study is to calculate natural frequencies and harmonic responses of cracked frames with general boundary conditions by using transfer matrix method (TMM). The TMM is a straightforward technique to obtain harmonic responses and natural frequencies of frame structures as the method is based on constructing a relationship between state vectors of two ends of structure by a chain multiplication procedure. A single variable shear deformation theory (SVSDT) is applied, as well as, Timoshenko beam theory (TBT) and Euler-Bernoulli beam theory (EBT) for comparison purposes. Firstly, free vibration analysis of intact and cracked frames are performed for different crack ratios using TMM. The crack is modelled by means of a linear rotational spring that divides frame members into segments. The results are verified by experimental data and finite element method (FEM) solutions. The harmonic response curves that represent resonant and anti-resonant frequencies directly are plotted for various crack lengths. It is seen that the TMM can be used effectively for harmonic response analysis of cracked frames as well as natural frequencies calculation. The results imply that the SVSDT is an efficient alternative for investigation of cracked frame vibrations especially with thick frame members. Moreover, EBT results can easily be obtained by ignoring shear deformation related terms from governing equation of motion of SVSDT.

Keywords: cracked frame; free vibration; harmonic response; single variable shear deformation theory; transfer matrix method

1. Introduction

The loss of stiffness due to structural damage affects the dynamic behavior of frame structures. Natural frequencies and harmonic responses of cracked frames are used as effective tools for non-destructive structural health monitoring of existing structures. From this point of view, accuracy of free and forced vibration analysis of cracked frames plays a very important role on taking precautions against catastrophic failures of engineering structures. The free vibration analysis of different types of cracked beams with various boundary conditions was well studied by many researchers (Ostachowicz and Krawczuk 1991, Chondros *et al.* 1998, Khiem and Lien 2001, Khiem and Lien 2004, Loya *et al.* 2006, Barad *et al.* 2013, Khiem and Toan 2014, Kindova-Petrova 2014, Thalapil and Maiti 2014, Khnaijar and Benamar 2017, Satpute *et al.* 2017, Elshamy *et al.* 2018, Khatir *et al.* 2018, Kim *et al.* 2018, Moezi *et al.* 2018). However, there are limited papers about vibrations of cracked frame structures in comparison with cracked beams. Nikolakopoulos *et al.* (1997) presented a crack identification procedure for a single-bay single-story frame model using FEM and experimentally obtained eigen frequencies. Brasiliano *et al.* (2004) applied residual error method in the moving equation for damage identification in frame structures. Carden and Fanning (2004) reviewed vibration based structural health monitoring techniques for beam-like structures. Umar *et al.* (2018) applied response surface methodology for crack detection of a steel portal frame. Due to complicated and time-consuming formulations, very few studies about exact vibrations of cracked frames can be found in literature. Greco and Pau (2012) performed free vibration analysis of cracked frames using EBT and dynamic stiffness formulations. Caddemi and Calio (2013) proposed a closed form solution for free vibration analysis of multiple-cracked single-bay single-story frame according to EBT via dynamic stiffness method (DSM). Labib *et al.* (2014) applied DSM to free vibrations of multiple-cracked frames using EBT. Ntakpe *et al.* (2014) investigated forward and inverse problem of cracked L-frames based on analytical solutions. The free vibration analysis results were compared with FEM solutions and a crack detection approach that based on a relation between strain energy for the transverse modes and natural frequency change due to damage was proposed. Free vibration of cracked beams was further studied by many authors, e.g. Tan *et al.* (2017) using Timoshenko beams, Shahverdi and Navardi (2017) using generalized differential quadrature element method and Cunedioglu (2015) for

*Corresponding author, Professor, Ph.D.
E-mail: magd.abdelwahab@tdtu.edu.vn
[a] Ph.D. candidate,
E-mail: baran.bozyigit@deu.edu.tr
[b] Associate Professor, Ph.D.
E-mail: yusuf.yesilce@deu.edu.tr

ISSN: 1225-4568 (Print), 1598-6217 (Online)

functionally graded sandwich beams. Moreover, the use of vibration data for damage assessment and structural health monitoring has been extensively used in the literature, e.g. Khatir *et al*. (2019), Tiachacht *et al*. (2018), Gillich *et al*. (2019).

Exact vibration analyses of cracked beam-like structures are generally performed by using a rotational spring to model the crack (Ostachowicz and Krawczuk 1991, Khiem and Lien 2001, Khiem and Lien 2004, Barad *et al.* 2013, Khiem and Toan 2014, Kindova-Petrova 2014). As equivalent rotational spring approach divides the cracked member into segments, the TMM is a perfect tool for performing free and forced vibration analyses of cracked beam-like structures. The TMM is based on obtaining the relation between state vectors of boundaries by a chain multiplication of transfer matrices of each segments. After construction of global transfer matrix of whole vibrating system, natural frequencies and harmonic responses can be calculated precisely. In recent years, the TMM was applied to free vibration analysis of various types of cracked beams with different boundary conditions (Attar 2012, Attar *et al.* 2014, Lee and Lee 2017, Lee and Lee 2017, Dastjerdi and Abbasi 2019).

It is seen from literature that, for the exact cracked frame vibration problem, the members were modelled as Euler-Bernoulli beams to simplify the complicated problem. However, it is well known that EBT overestimates natural frequencies of thick beams due to the assumption of cross-sections of beams remain rigid and perpendicular to beam axis under bending. Thus, an important task about using more realistic beam theories on exact free and forced vibrations of cracked frames arises. The TBT is an important alternative as the theory does not ignore shear deformation and rotation inertia. Anagnostides (1986) used dynamic stiffness formulations for harmonic response analysis of single-bay single-story space frame. However, there is a shear coefficient parameter based on cross-section geometries for reducing the error of assuming constant shear stress distribution on the cross-section (Han *et al.* 1999). Thus, high-order beam theories that focus on realistic shear stress distribution on cross-sections were studied (Levinson 1981, Bickford 1982, Heyliger and Reddy 1988). Although high-order beam theories provide more realistic results in comparison with EBT and TBT, the formulations of high-order beam theories and their use for beam-assembly structures such as frames are not effectively applicable. Therefore, a research area focusing on a simple, effective and realistic beam theory arised. Shimpi *et al.* (2017) presented a new SVSDT, which considered a parabolic shear stress distribution along cross-section. Bozyigit and Yesilce (2018) investigated free vibrations and harmonic responses of multi-story frames using SVSDT via DSM. The SVSDT does not require a shear coefficient factor and formulations of SVSDT are applicable to vibrations of frame structures as equation of motion is a fourth order differential equation similar to EBT and TBT. Another important advantage of SVSDT is that it provides EBT results as a special case by ignoring terms of shear deformation from governing equation of motion (Shimpi *et al.* 2017).

In recent years, isogeometric analysis (IGA), which outweighs classical FEM in terms of high differentiability was used as an effective tool for solving novel three-variable plate formulations (Nguyen *et al.* 2017) and applied to static analysis of laminated composite plates using high order shear deformation theory (Nguyen *et al.* 2016). The quasi-3D IGA was performed for functionally graded micro plates based on modified coupled stress theory (Nguyen *et al.* 2017) and for size-dependent analysis of functionally graded nanoplates (Nguyen *et al*. 2015). The IGA can be an important alternative for the analysis of cracked structures. An extended IGA was applied to thin shell analysis based on Kirchhoff-Love theory (Nguyen-Thanh *et al.* 2015).

Accurate analysis of cracked structures is not limited by simple crack modeling approaches like equivalent spring method. Areias *et al*. (2016) introduced a new staggered algorithm for elastic materials using a phase-model of crack regularization. Rabczuk *et al*. (2007) used crack particles and local partition of unity techniques to model cracks in continua. Areias and Rabczuk (2013) investigated finite strain fractures of plates and shells considering brittle fracture where energy is dissipated in a crack edge and quasi-brittle fracture where energy is dissipated in a surface. Rabczuk *et al*. (2010) treated cracks of a structure conveying fluid by introducing either cracking particle method and partition of unity base method, which is continuous discontinuities into the approximation. Recently, the extended IGA (XIGA), which is the combination of IGA and extended FEM, was applied to crack detection and quantification of plate structures (Khatir and Abdel Wahab 2019). Khatir *et al*. (2019) presented a study on the use of modal strain energy damage indicator coupled with teaching-learning-based optimization algorithm and IGA.

In this study, free and forced vibration analyses of cracked frames are investigated by using SVSDT via transfer matrix formulations. Firstly, natural frequencies of a L-type frame are calculated for experimental validation of results. Then, a numerical case study of a single-bay single-story cracked frame is presented for general boundary conditions, which are fixed-fixed (F-F), fixed-simple (F-S) and simple-simple (S-S). First three natural frequencies of frame model using SVSDT are presented comparatively with TBT and EBT results. Moreover, FEM solutions of SAP2000 are also tabulated with TMM results for validation. Finally, harmonic response curves of single-bay single-story frame model are plotted for various crack length values by using bending moment and shear force response of supports. The novelties of this study are based on performing forced vibration analysis of a frame structure by using TMM and applying a novel beam theory other than EBT and TBT to vibrations of cracked frames.

This paper consists of six main sections. After the introduction, the second section presents details of SVSDT formulations for bending vibration, formulations of axial vibration and crack modelling approach. Application of TMM on free and forced vibrations of cracked frames are presented in the third section. In the fourth section, the numerical free vibration results of proposed approach is validated by using experimental data from literature. Section five illustrates three numerical case studies

considering general boundary conditions. The paper is finalized with concluding remarks in section six.

2. Theory and model

The following assumptions are considered in this study:

1. The material of frame members is isotropic.
2. The cross-sections of frame members is uniform.
3. The behavior of frame is linear elastic.
4. The cracks remain open during the vibration of structure.
5. The damping is neglected for simplification.

The foundation of SVSDT formulations are based on bending and shearing components of transverse displacement of the beam as (Shimpi *et al.* 2017):

$$y^T = y_b + y_s \tag{1}$$

where y^T represents the total transverse displacement, y_b and y_s represent the bending and shearing components of transverse displacement, respectively. According to SVSDT, the governing equation of motion of a beam in free vibration can be written as (Shimpi *et al.* 2017):

$$\begin{aligned} &EI\frac{\partial^4 y_b}{\partial x^4} - \frac{\bar{m}I}{A}\left(1+\frac{12(1+\nu)}{5}\right)\frac{\partial^4 y_b}{\partial x^2 \partial t^2} \\ &+\bar{m}\frac{\partial^2 y_b}{\partial t^2} + \frac{\bar{m}^2 I}{A^2 E}\frac{12(1+\nu)}{5}\frac{\partial^4 y_b}{\partial t^4} = 0 \end{aligned} \tag{2}$$

where x is coordinate, t is time, E is elastic modulus, A is area of cross-section, I is area moment of inertia, ν is Poisson's ratio and $\bar{m}$ is mass per unit lentgh. The component y_b is obtained from the solution of Eq.(2). Eq.(3) is obtained with the assumption of $y_b(x,t) = y_b(x)e^{i\omega t}$ where ω and i represent natural frequency and imaginary unit, respectively. Applying separation of variables technique for the beam having a length L gives,

$$A_0\frac{d^4 y_b}{dz^4} + B_0\omega^2\frac{d^2 y_b}{dz^2} - C_0\omega^2 y_b(z) + D_0\omega^4 y_b(z) = 0 \tag{3}$$

where

$$A_0 = EI/L^4; B_0 = -\bar{m}I/AL^2\left(1+\frac{12(1+\nu)}{5}\right);$$
$$C_0 = \bar{m}; D_0 = \bar{m}^2 I\left(\frac{12(1+\nu)}{5}\right)/A^2E; z = x/L$$

It should be noted that A_0, B_0, C_0 and D_0 are notations used for a clear presentation of equation and they do not have physical meaning.

The solution of $y_b(z)$ is written as (Bozyigit and Yesilce 2018):

$$y_b(z) = \{D\}e^{ikz} \tag{4}$$

$y_b(z)$ can be written in open form in Eq.(5) as assembly of four components as Eq.(3) is a fourth order ordinary differential equation.

$$y_b(z) = (D_1e^{ik_1z} + D_2e^{ik_2z} + D_3e^{ik_3z} + D_4e^{ik_4z}) \tag{5}$$

where D_1, D_2, D_3, D_4 are integration constants and k_1, k_2, k_3, k_4 are characteristic roots that obtained from the solution of Eq.(3). The following procedure is used for calculation of characteristic roots: Eq.(4) is substituted into Eq.(3) and derivation of fourth order (first term in left-hand side of Eq.(3)) and second order (second term in left-hand side of Eq.(3)) are obtained. Then, a fourth order equation with unknown k is achieved. The solution of the fourth order equation provides four characteristic roots which are k_1, k_2, k_3 and k_4.

By using Eq.(5), the bending component of slope function according to SVSDT is written as:

$$\frac{dy_b}{dz} = (ik_1D_1e^{ik_1z} + ik_2D_2e^{ik_2z} + ik_3D_3e^{ik_3z} + ik_4D_4e^{ik_4z}) \tag{6}$$

The bending moment function and shear force function according to SVSDT are presented in Eqs. (7) and (8), respectively (Shimpi *et al.* 2017).

$$M(z) = -\frac{EI}{L^2}\frac{d^2 y_b}{dz^2} \tag{7}$$

$$Q(z) = -\frac{EI}{L^3}\frac{d^3 y_b}{dz^3} - \frac{\bar{m}I\omega^2}{AL}\frac{dy_b}{dz} \tag{8}$$

where $M(z)$ and $Q(z)$ represent bending moment function and shear force function, respectively. Eqs. (7)-(8) are rewritten as Eqs.(9)-(10) using Eq. (5) as

$$\begin{aligned} M(z) = (&Hk_1^2D_1e^{ik_1z} + Hk_2^2D_2e^{ik_2z} \\ &+Hk_3^2D_3e^{ik_3z} + Hk_4^2D_4e^{ik_4z}) \end{aligned} \tag{9}$$

$$\begin{aligned} Q(z) = &(Jik_1^3 - Kik_1)D_1e^{ik_1z} + (Jik_2^3 - Kik_2)D_2e^{ik_2z} \\ &+(Jik_3^3 - Kik_3)D_3e^{ik_3z} + (Jik_4^3 - Kik_4)D_4e^{ik_4z} \end{aligned} \tag{10}$$

where

$$K = (\bar{m}I\omega^2)/(AL), H = EI/L^2, J = EI/L^3$$

It should be noted that H, J and K are notations for a simple representation of internal force functions.

The shearing component of transverse displacement function and total transverse displacement function are given in Eqs. (11) and (12), respectively (Shimpi *et al.* 2017).

$$y_s = T\left(-H\frac{d^2 y_b}{dz^2} - Py_b(z)\right) \tag{11}$$

$$\begin{aligned} y^T = &\left(THk_1^2 - TP + 1\right)D_1e^{ik_1z} + \left(THk_2^2 - TP + 1\right)D_2e^{ik_2z} \\ &+\left(THk_3^2 - TP + 1\right)D_3e^{ik_3z} + \left(NHk_4^2 - TP + 1\right)D_4e^{ik_4z} \end{aligned} \tag{12}$$

where

$$T = 12(1+\nu)/5AE; P = \left(\bar{m}I\omega^2/A\right)$$

The total slope function can be written as assembly of bending and shearing components of slope:

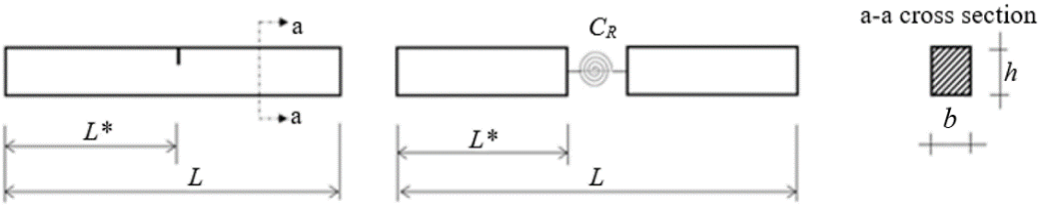

Fig. 1 A single cracked frame member modeled by a linear rotational spring

$$\frac{dy^T}{dz} = \left(ik_1 + TJik_1^3 - TRik_1\right)D_1e^{ik_1z} + \left(ik_2 + TJik_2^3 - TRik_2\right)D_2e^{ik_2z} + \left(ik_3 + TJik_3^3 - TRik_3\right)D_3e^{ik_3z} + \left(ik_4 + TJik_4^3 - TRik_4\right)D_4e^{ik_4z} \quad (13)$$

where the notation R is defined as $R=P/L$ for simplification.

In this study, the axial vibrations of frame members are considered. Thus, axial displacement and axial force functions of members are obtained by solving the equation of motion of a beam in free axial vibration (Rao 1995):

$$AE\frac{\partial^2 u(x,t)}{\partial x^2} - \bar{m}\frac{\partial^2 u(x,t)}{\partial t^2} = 0 \quad (14)$$

where $u(x,t)$ is axial displacement function. Eq.(15) can be obtained by assuming $u(x,t)=u(x)e^{i\omega t}$ and applying separation of variables method.

$$\frac{d^2u(z)}{dz^2} + \frac{\bar{m}\omega^2L^2}{AE}u(z) = 0 \quad (15)$$

The axial displacement function and axial force function of frame members are obtained by substituting Eq.(16) into Eq.(15) as Eqs.(17)-(18), respectively.

$$u(z) = \{D\}e^{ikz} \quad (16)$$

$$u(z) = (D_5e^{ik_5z} + D_6e^{ik_6z}) \quad (17)$$

$$N(z) = V(ik_5D_5e^{ik_5z} + ik_6D_6e^{ik_6z}) \quad (18)$$

where D_5, D_6 are integration constants and k_5, k_6 are characteristic roots that calculated from the solution of Eq.(15) and V is defined as $V=AE/L$ for simplification.

The crack modelling approach of this study is using a linear rotational spring for representing local stiffness reduce. A single cracked frame member modelled by means of a linear rotational spring is presented in Fig. 1 where C_R represents spring flexibility, b represents width of the cross section, h represents height of the cross section, L^* and L represent location of crack and length of the frame member, respectively.

The C_R constant can be calculated via Eqs. (19)-(20) as (Ostachowicz and Krawczuk 1991):

$$C_R = \frac{72\pi f(\alpha)}{Ebh^2} \quad (19)$$

$$f(\alpha) = 0.6384\alpha^2 - 1.035\alpha^3 + 3.7201\alpha^4 - 5.1773\alpha^5 + 7.553\alpha^6 - 7.332\alpha^7 + 2.4909\alpha^8 \quad (20)$$

where α is crack ratio (l_c/h), l_c is crack length and $f(\alpha)$ is local compliance function calculated according to linear elastic fracture mechanics (Kindova-Petrova 2014). The TMM procedures according to SVSDT can be started by using Eqs.(9)-(10), Eqs.(12)-(13) and Eqs.(17)-(20).

3. Transfer matrix formulations

The transfer matrix of a frame member can be formed using the relation between internal forces and displacements at two ends ($z=0$ and $z=1$). The state vector (Z) of left-hand side ($z=0$) is given as:

$$\begin{Bmatrix} u \\ y^T \\ \frac{dy^T}{dz} \\ N \\ Q \\ M \end{Bmatrix}_{z=0} = \begin{bmatrix} 0 & 0 & 0 & 0 & 1 & 1 \\ \lambda_1 & \lambda_2 & \lambda_3 & \lambda_4 & 0 & 0 \\ \eta_1 & \eta_2 & \eta_3 & \eta_4 & 0 & 0 \\ 0 & 0 & 0 & 0 & Vik_5 & Vik_6 \\ \kappa_1 & \kappa_2 & \kappa_3 & \kappa_4 & 0 & 0 \\ \varsigma_1 & \varsigma_2 & \varsigma_3 & \varsigma_4 & 0 & 0 \end{bmatrix} \begin{Bmatrix} D_1 \\ D_2 \\ D_3 \\ D_4 \\ D_5 \\ D_6 \end{Bmatrix} \quad (21)$$

where

$$\lambda_n = \left(THk_n^2 - TP + 1\right), \eta_n = \left(ik_n + TJik_n^3 - TRik_n\right),$$
$$\kappa_n = (Jik_n^3 - Kik_n), \varsigma_n = Hk_n^2, (n = 1,2,3,4)$$

Eq.(21) is rewritten in closed form as

$$\{Z\}_{z=0} = [T_0]\{D\} \quad (22)$$

where

$$[T_0] = \begin{bmatrix} 0 & 0 & 0 & 0 & 1 & 1 \\ \lambda_1 & \lambda_2 & \lambda_3 & \lambda_4 & 0 & 0 \\ \eta_1 & \eta_2 & \eta_3 & \eta_4 & 0 & 0 \\ 0 & 0 & 0 & 0 & Vik_5 & Vik_6 \\ \kappa_1 & \kappa_2 & \kappa_3 & \kappa_4 & 0 & 0 \\ \varsigma_1 & \varsigma_2 & \varsigma_3 & \varsigma_4 & 0 & 0 \end{bmatrix}$$

The state vector of right-hand side (z=1) of frame member element is given in Eq. (23).

$$\begin{Bmatrix} u \\ y^T \\ \frac{dy^T}{dz} \\ N \\ Q \\ M \end{Bmatrix}_{z=1} = \begin{bmatrix} 0 & 0 & 0 & 0 & e^{ik_5} & e^{ik_6} \\ e^{ik_1}\lambda_1 & e^{ik_2}\lambda_2 & e^{ik_3}\lambda_3 & e^{ik_4}\lambda_4 & 0 & 0 \\ e^{ik_1}\eta_1 & e^{ik_2}\eta_2 & e^{ik_3}\eta_3 & e^{ik_4}\eta_4 & 0 & 0 \\ 0 & 0 & 0 & 0 & e^{ik_5}Vik_5 & e^{ik_6}Vik_6 \\ e^{ik_1}\kappa_1 & e^{ik_2}\kappa_2 & e^{ik_3}\kappa_3 & e^{ik_4}\kappa_4 & 0 & 0 \\ e^{ik_1}\varsigma_1 & e^{ik_2}\varsigma_2 & e^{ik_3}\varsigma_3 & e^{ik_4}\varsigma_4 & 0 & 0 \end{bmatrix} \begin{Bmatrix} D_1 \\ D_2 \\ D_3 \\ D_4 \\ D_5 \\ D_6 \end{Bmatrix} \quad (23)$$

Eq. (23) can be formed in a simple form as:

$$\{Z\}_{z=1} = [T_l]\{D\} \tag{24}$$

where

$$[T_1] = \begin{bmatrix} 0 & 0 & 0 & 0 & e^{ik_5} & e^{ik_6} \\ e^{ik_1}\lambda_1 & e^{ik_2}\lambda_2 & e^{ik_3}\lambda_3 & e^{ik_4}\lambda_4 & 0 & 0 \\ e^{ik_1}\eta_1 & e^{ik_2}\eta_2 & e^{ik_3}\eta_3 & e^{ik_4}\eta_4 & 0 & 0 \\ 0 & 0 & 0 & 0 & Vik_5 e^{ik_5} & Vik_6 e^{ik_6} \\ e^{ik_1}\kappa_1 & e^{ik_2}\kappa_2 & e^{ik_3}\kappa_3 & e^{ik_4}\kappa_4 & 0 & 0 \\ e^{ik_1}\varsigma_1 & e^{ik_2}\varsigma_2 & e^{ik_3}\varsigma_3 & e^{ik_4}\varsigma_4 & 0 & 0 \end{bmatrix} \tag{25}$$

$\{D\}$ is written as Eqs. (25) and (26) using Eqs.(21) and (23), respectively.

$$\{D\} = [T_0]^{-1}\{Z\}_{z=0} \tag{25}$$

$$\{D\} = [T_1]^{-1}\{Z\}_{z=1} \tag{26}$$

By using Eqs. (25)-(26), the relation between state vectors $\{Z\}_{z=0}$ and $\{Z\}_{z=1}$ can be obtained as:

$$\{Z\}_{z=1} = [T_1]\,[T_0]^{-1}\{Z\}_{z=0} \tag{27}$$

$$\{Z\}_{z=1} = [T^*]\{Z\}_{z=0} \tag{28}$$

where $[T^*]=[T_1]\,[T_0]^{-1}$ and $[T^*]$ represents local transfer matrix of beam element.

The global transfer matrix of frame members are constructed using angular transformation of local transfer matrices. The angular transformation matrix (ATM) and global transfer matrix of a frame member are given in Eqs. (29) and Eq. (30), respectively.

$$[ATM] = \begin{bmatrix} \cos(\theta) & \sin(\theta) & 0 & 0 & 0 & 0 \\ -\sin(\theta) & \cos(\theta) & 0 & 0 & 0 & 0 \\ 0 & 0 & 1 & 0 & 0 & 0 \\ 0 & 0 & 0 & \cos(\theta) & \sin(\theta) & 0 \\ 0 & 0 & 0 & -\sin(\theta) & \cos(\theta) & 0 \\ 0 & 0 & 0 & 0 & 0 & 1 \end{bmatrix} \tag{29}$$

$$[T_G^*] = [ATM]^{-1}[T^*][ATM] \tag{30}$$

where, θ represents angle between local axes of the frame member and global axes of the frame, $[T_G^*]$ is the global transfer matrix of frame member modelled according to SVSDT. It should be noted that global axes of all frame models in this study are taken as local axes of horizontal frame member. Therefore, θ is taken as 0.5π radian and 0 radian for all column members and beam members, respectively.

If the frame member is divided into m sub-segments along its length, the global transfer matrix of the system can be obtained by a chain multiplication of transfer matrices of frame segments as:

$$[T_{FR}^*] = [T_{G,m}^*][T_{G,m-1}^*]\cdots[T_{G,2}^*][T_{G,1}^*] \tag{31}$$

where $[T_{FR}^*]$ is global transfer matrix of frame structure.

Table 1 Reduced global transfer matrices of frames for general boundary conditions

Boundary condition	Reduced global transfer matrix
Simple-Simple	$\begin{bmatrix} T_{FR}^*(1,3) & T_{FR}^*(1,4) & T_{FR}^*(1,5) \\ T_{FR}^*(2,3) & T_{FR}^*(2,4) & T_{FR}^*(2,5) \\ T_{FR}^*(6,3) & T_{FR}^*(6,4) & T_{FR}^*(6,5) \end{bmatrix}$
Fixed-Simple	$\begin{bmatrix} T_{FR}^*(1,4) & T_{FR}^*(1,5) & T_{FR}^*(1,6) \\ T_{FR}^*(2,4) & T_{FR}^*(2,5) & T_{FR}^*(2,6) \\ T_{FR}^*(6,4) & T_{FR}^*(6,5) & T_{FR}^*(6,6) \end{bmatrix}$
Fixed-Fixed	$\begin{bmatrix} T_{FR}^*(1,4) & T_{FR}^*(1,5) & T_{FR}^*(1,6) \\ T_{FR}^*(2,4) & T_{FR}^*(2,5) & T_{FR}^*(2,6) \\ T_{FR}^*(3,4) & T_{FR}^*(3,5) & T_{FR}^*(3,6) \end{bmatrix}$
Fixed-Free	$\begin{bmatrix} T_{FR}^*(4,4) & T_{FR}^*(4,5) & T_{FR}^*(4,6) \\ T_{FR}^*(5,4) & T_{FR}^*(5,5) & T_{FR}^*(5,6) \\ T_{FR}^*(6,4) & T_{FR}^*(6,5) & T_{FR}^*(6,6) \end{bmatrix}$

A discontinuity occurs between slopes of frame member segments as a result of using a rotational spring for crack modelling. Thus, an additional local flexibility matrix that represents the discontinuity at crack location is added in Eq.(31). The global transfer matrix of the cracked frame can be constructed using Eq. (31) and local flexibility matrix $[C^*]$ where

$$[C^*] = \begin{bmatrix} 1 & 0 & 0 & 0 & 0 & 0 \\ 0 & 1 & 0 & 0 & 0 & 0 \\ 0 & 0 & 1 & 0 & 0 & C_R \\ 0 & 0 & 0 & 1 & 0 & 0 \\ 0 & 0 & 0 & 0 & 1 & 0 \\ 0 & 0 & 0 & 0 & 0 & 1 \end{bmatrix}$$

3.1 Free vibration analysis

One of the main advantages of TMM on free vibration analysis of beam-assembly structures such as frames is that dimensions of reduced global transfer matrix remain 3×3 independently from number of frame member segments and any other local attachments. After construction of global transfer matrix written in Eq. (31), a reduction procedure according to boundary conditions is applied. The reduced global transfer matrices of frames for general boundary conditions are given in Table 1.

In Table 1, $T_{FR}^*(i,j)$ (i=1:6; j=3:6) represents the reduced global transfer matrix member, which is located at i^{th} row and j^{th} column of global transfer matrix of frame.

The ω values equating the determinant of reduced global transfer matrices to zero are obtained as natural frequencies for intact and cracked frame models. A trial and error procedure based on interpolation is used for calculating roots. When there is a change of sign between trial values, there must be a root lying in this interval. Using some iterations, the natural frequencies can be calculated. The calculation of natural frequencies is performed in MATLAB.

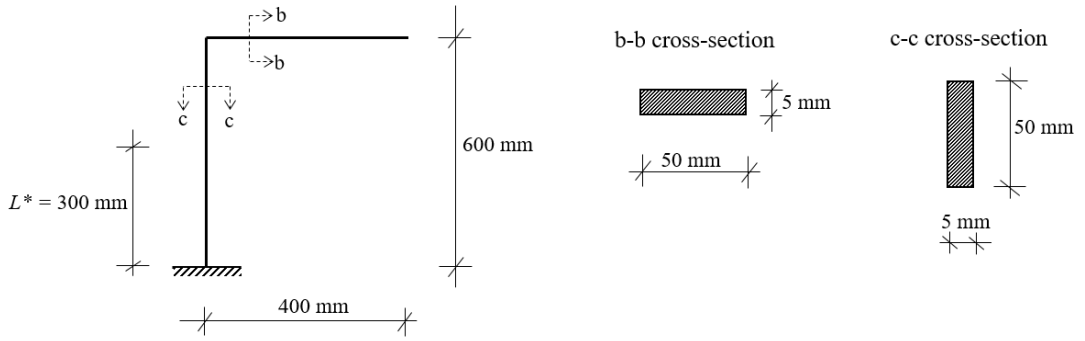

Fig. 2 Cracked L-type frame model with geometric properties

3.2 Forced vibration analysis

The transfer matrix formulations of state vectors presented in Eqs.(21) and (23) are reformed as Eqs.(32) and (33), respectively.

$$\begin{Bmatrix} 1 \\ u \\ y^T \\ \dfrac{dy^T}{dz} \\ N \\ Q \\ M \end{Bmatrix}_{z=0(\ forced\ )} = \begin{bmatrix} 1 & 0 & 0 & 0 & 0 & 0 & 0 \\ 0 & 0 & 0 & 0 & 0 & 1 & 1 \\ 0 & \lambda_1 & \lambda_2 & \lambda_3 & \lambda_4 & 0 & 0 \\ 0 & \eta_1 & \eta_2 & \eta_3 & \eta_4 & 0 & 0 \\ 0 & 0 & 0 & 0 & 0 & Vik_5 & Vik_6 \\ 0 & \kappa_1 & \kappa_2 & \kappa_3 & \kappa_4 & 0 & 0 \\ 0 & \varsigma_1 & \varsigma_2 & \varsigma_3 & \varsigma_4 & 0 & 0 \end{bmatrix} \begin{Bmatrix} 1 \\ D_1 \\ D_2 \\ D_3 \\ D_4 \\ D_5 \\ D_6 \end{Bmatrix} \quad (32)$$

$$\begin{Bmatrix} 1 \\ u \\ y^T \\ \dfrac{dy^T}{dz} \\ N \\ Q \\ M \end{Bmatrix}_{z=1(\ forced\ )} = \begin{bmatrix} 1 & 0 & 0 & 0 & 0 & 0 & 0 \\ 0 & 0 & 0 & 0 & 0 & e^{ik_5} & e^{ik_6} \\ 0 & e^{ik_1}\lambda_1 & e^{ik_2}\lambda_2 & e^{ik_3}\lambda_3 & e^{ik_4}\lambda_4 & 0 & 0 \\ 0 & e^{ik_1}\eta_1 & e^{ik_2}\eta_2 & e^{ik_3}\eta_3 & e^{ik_4}\eta_4 & 0 & 0 \\ 0 & 0 & 0 & 0 & 0 & e^{ik_5}Vik_5 & e^{ik_6}Vik_6 \\ 0 & e^{ik_1}\kappa_1 & e^{ik_2}\kappa_2 & e^{ik_3}\kappa_3 & e^{ik_4}\kappa_4 & 0 & 0 \\ 0 & e^{ik_1}\varsigma_1 & e^{ik_2}\varsigma_2 & e^{ik_3}\varsigma_3 & e^{ik_4}\varsigma_4 & 0 & 0 \end{bmatrix} \begin{Bmatrix} 1 \\ D_1 \\ D_2 \\ D_3 \\ D_4 \\ D_5 \\ D_6 \end{Bmatrix} \quad (33)$$

As matrix dimensions must agree for mathematical formulations of TMM, the angular transformation matrix and local flexibility matrix of crack location are revised as Eqs. (34) and (35), respectively.

$$[ATM]_{forced} = \begin{bmatrix} 1 & 0 & 0 & 0 & 0 & 0 & 0 \\ 0 & \cos(\theta) & \sin(\theta) & 0 & 0 & 0 & 0 \\ 0 & -\sin(\theta) & \cos(\theta) & 0 & 0 & 0 & 0 \\ 0 & 0 & 0 & 1 & 0 & 0 & 0 \\ 0 & 0 & 0 & 0 & \cos(\theta) & \sin(\theta) & 0 \\ 0 & 0 & 0 & 0 & -\sin(\theta) & \cos(\theta) & 0 \\ 0 & 0 & 0 & 0 & 0 & 0 & 1 \end{bmatrix} \quad (34)$$

$$[C^*] = \begin{bmatrix} 1 & 0 & 0 & 0 & 0 & 0 & 0 \\ 0 & 1 & 0 & 0 & 0 & 0 & 0 \\ 0 & 0 & 1 & 0 & 0 & 0 & 0 \\ 0 & 0 & 0 & 1 & 0 & 0 & C_R \\ 0 & 0 & 0 & 0 & 1 & 0 & 0 \\ 0 & 0 & 0 & 0 & 0 & 1 & 0 \\ 0 & 0 & 0 & 0 & 0 & 0 & 1 \end{bmatrix} \quad (35)$$

Finally, a jump matrix with dimensions 7×7 is defined for a beam-column joint of frame structure under a dynamic point load as:

$$[F_J] = \begin{bmatrix} 1 & 0 & 0 & 0 & 0 & 0 & 0 \\ 0 & \cos(\theta) & \sin(\theta) & 0 & 0 & 0 & 0 \\ 0 & -\sin(\theta) & \cos(\theta) & 0 & 0 & 0 & 0 \\ 0 & 0 & 0 & 1 & 0 & 0 & 0 \\ 0 & 0 & 0 & 0 & \cos(\theta) & \sin(\theta) & 0 \\ P_0 & 0 & 0 & 0 & -\sin(\theta) & \cos(\theta) & 0 \\ 0 & 0 & 0 & 0 & 0 & 0 & 1 \end{bmatrix} \quad (36)$$

where P_0 and $[F_J]$ represent the amplitude of point dynamic load and the jump matrix of node under dynamic load, respectively. The use of $[F_J]$ is necessary to reflect the discontinuity of beam-column joint under dynamic point load. Eq.(36) is constructed as a special case of standard angular transformation matrix by adding dynamic load parameter.

The harmonic response curves of cracked frames can be plotted using the global transfer matrix of system that constructed by a chain of matrix multiplication using Eqs. (32)-(36). By ignoring first row and first column of global transfer matrix for forced vibration analysis, a 6×6 matrix that represents relationship between supports of frame structure is obtained. The harmonic responses of supports can be calculated with ease by solving a 6×6 system of equations with known zero displacements and zero forces according to boundary conditions.

It should be noted that the detailed TMM formulations for free and forced vibrations of cracked frames using well known EBT and TBT are not presented to shorten the paper. A brief summarized formulation of EBT and TBT for transfer matrix formulations can be found in Appendix section.

4. Comparison of TMM results and experimental data

Due to lack of experimental studies based on cracked frame structures, a L-type frame model is considered. The natural frequencies of a cracked L-type frame presented in Fig. 2 are calculated via the proposed approach. The first four natural frequencies of L-type frame model are

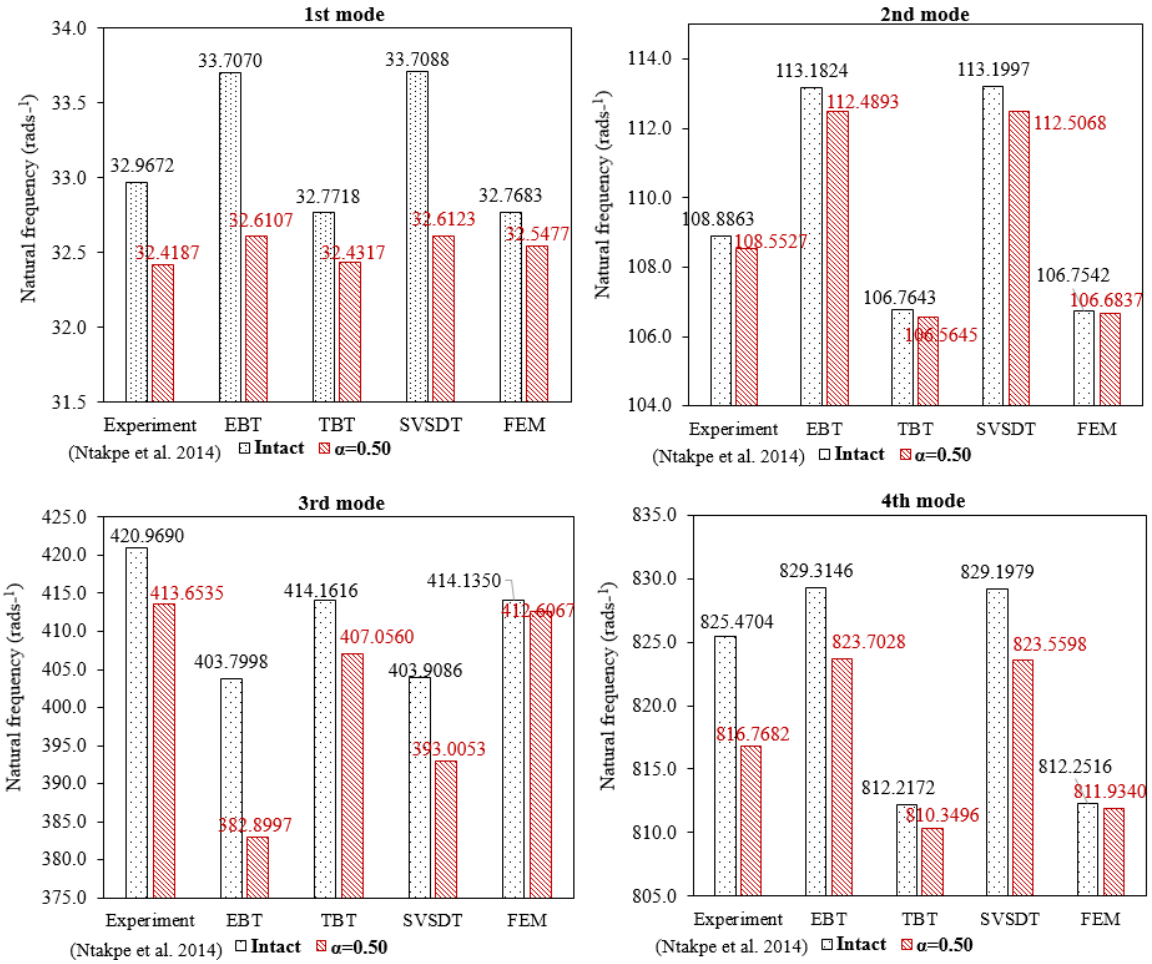

Fig. 3 First four natural frequencies of L-type frame model

presented in Fig.3. Furthermore, Fig.4 represents fifth, sixth, seventh and eighth natural frequencies of L-type frame. The following material properties are considered: Mass density = 7850 kg/m^3, ν = 0.3, E = 2×10^{11} N/m^2. For the experiment, the crack was made by a saw cut, which has a width of 2 mm (Ntakpe *et al.* 2014).

Figs.3-4 show that TMM results on free vibration analysis of cracked L-type frames are in a good agreement with experimental data. All of the first eight natural frequencies are decreased by a crack having 2.5 mm depth (α=0.50) for EBT, TBT and SVSDT. It is seen from Figs. 3 and 4 that SVSDT provides higher natural frequencies for 1st, 2nd, 4th and 7th modes, when compared to TBT. The relative errors between TMM approach and experimental modal analysis results on natural frequencies are presented in Table 2. According to Table 2, the maximum error of proposed approach is below 5% for natural frequencies calculation of frame model using SVSDT and TBT. This acceptable error level may be a result of non-ideal fixed support condition and non-exact material properties of experiment. Table 2 also reveals that the accuracy of TBT for cracked frame vibrations is higher than intact frame vibration. However, SVSDT provides more accurate natural frequencies for cracked frame in comparison with intact frame only for first two modes according to experimental results. The SVSDT should provide more realistic results in comparison with TBT according to theoretical assumptions. The SVSDT considers a parabolic shear stress distribution along cross-section. However, the height of cross-section of frame members used in experimental validation is very small (5 mm). Therefore, for the thin frame members used in the experiment, non-constant shear stress distribution on cross-sections may become insignificant and this situation may result in relatively high errors between SVSDT and experimental results.

It should be noted that FEM results in the experimental validation section of this study is based on meshing frame members in 250 segments. The convergence of FEM results of SAP2000 is presented in Fig. 5 for the first eight natural frequencies of L-type frame model. Moreover, the first eight mode shapes of intact L-type frame can be seen from Fig. 6 to observe symmetric and anti-symmetric modes. Fig.6 shows that the crack location is very close to a node on the fifth mode shape of L-type frame. Therefore, the effect of crack on natural frequencies is minimum for fifth mode of L-type frame model.

5. Numerical case study

A numerical example is presented for cracked single-bay single-story frame model with general boundary conditions, which are F-F, F-S and S-S. As frame structures

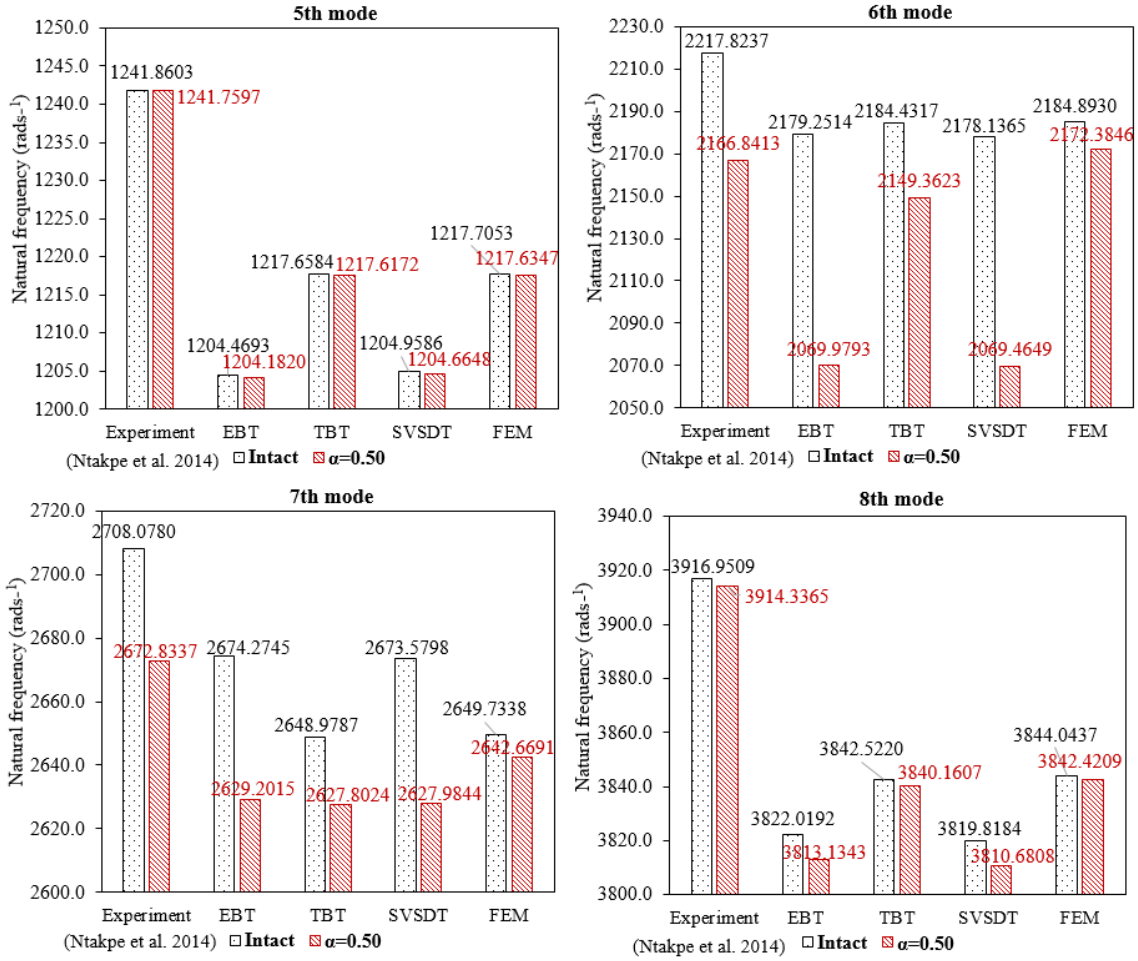

Fig. 4. Fifth, sixth, seventh and eighth natural frequencies of L-type frame model

in engineering applications are not limited to fixed supported building type frames, different combinations of boundary conditions are considered. The proposed approach can be used effectively for different boundary conditions using Table 1. The crack location and length of frame members can be observed from Fig. 7 where $P(t)$ and $\overline{\omega}$ represent a dynamic point load and forcing frequency, respectively. The numerical case study is based on the following data: ν = 0.2, mass density = 2500 kg/m^3, E = 2×10^{10} N/m^2, cross-sections of columns = 0.3 × 0.3 m, cross-sections of beams = 0.25 × 0.50 m.

The first three natural frequencies of intact frame models are presented in Table 3 using TMM and FEM. For different crack ratio values, Tables 4-6 list natural frequencies of cracked frames having S-S, F-S and F-F boundary conditions, respectively. It should be noted that FEM results of SAP2000 are based on the following crack modeling technique: Firstly, the cracked column is cut from crack location and a two joint link element is defined at this section. Then, the spring stiffness that calculated from Eqs. (19) and (20) is entered as effective rotational spring stiffness value of two joint link element. The other displacements of two joint link element except rotation are restrained to reflect the jump of rotation because of crack. A representation of cracked frame in SAP2000 can be seen in Fig. 8.

Table 2 The relative errors between proposed approach, FEM and experimental results

		Relative error (%)							
	Mode	1st	2nd	3rd	4th	5th	6th	7th	8th
Intact	EBT	2.24	3.95	4.08	0.47	3.01	1.74	1.25	2.42
	TBT	0.59	1.95	1.62	1.61	1.95	1.51	2.18	1.90
	SVSDT	2.25	3.96	4.05	0.45	2.97	1.79	1.27	2.48
	SAP2000	0.60	1.96	1.62	1.60	1.95	1.48	2.15	1.86
α=0.50	EBT	0.59	3.63	7.43	0.85	3.03	4.47	1.63	2.59
	TBT	0.04	1.83	1.59	0.79	1.94	0.81	1.68	1.89
	SVSDT	0.60	3.64	4.99	0.83	2.99	4.49	1.68	2.65
	SAP2000	0.40	1.72	0.25	0.59	1.94	0.26	1.13	1.84

According to Tables 3-6, EBT overestimates natural frequencies of single-bay single-story frame models. Table 3 shows that the SVSDT provides slightly higher natural frequencies in comparison with TBT for general boundary conditions of single-bay single-story intact frame.

Tables 3-6 reveal that highest natural frequencies are obtained from fixed supported frame and lowest natural frequencies are obtained from simply supported frame for EBT, SVSDT and TBT. For cracked single-bay single-story frame model, it can be seen from Tables 4-6 that increasing

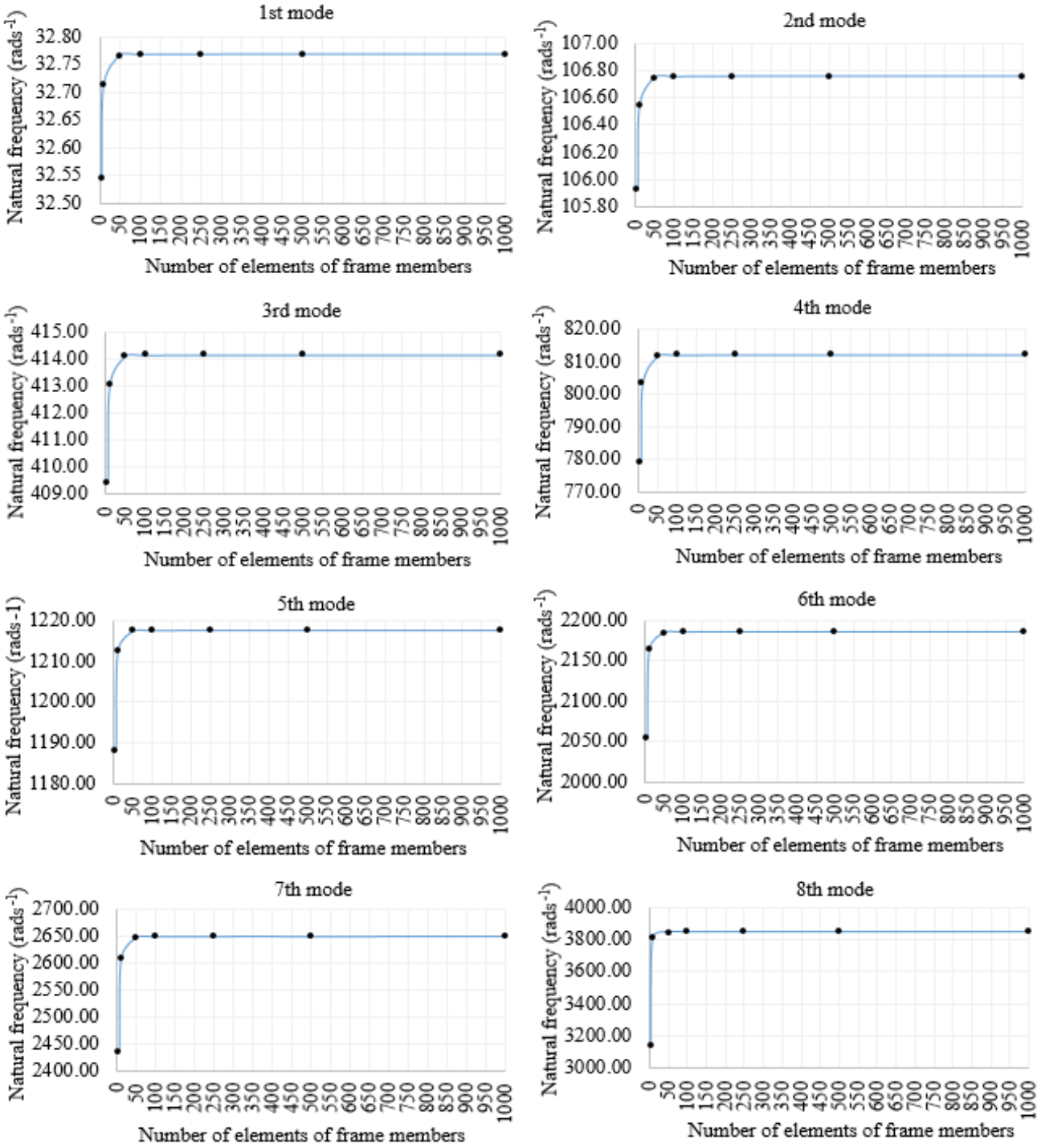

Fig. 5. FEM convergence for intact L-type frame model

crack ratio decreases natural frequencies for F-F, F-S as well as S-S boundary condition. According to Tables 4-6, the TMM results using SVSDT and TBT are in a good agreement with FEM results. The relative error between FEM results and TMM for intact and cracked single-bay single-story frames are tabulated in Table 7. According to Table 7, the maximum error between TMM formulations of SVSDT and FEM results of SAP2000 is below 4% on natural frequency calculation of frame models. It can be observed from Table 7 that relative errors on natural frequencies between TBT and FEM are lower than relative error between SVSDT and FEM because SAP2000 uses a similar beam modelling approach like TBT.

It should be noted that FEM results in the numerical case study is obtained by meshing members of single-bay single-story frame models in 250 segments to obtain a perfect convergence. The convergence of FEM results of SAP2000 can be seen from Fig.9 for first three natural frequencies for S-S, F-S and F-F boundary conditions.

The first three mode shapes of intact single-span single-story frame models can be seen from Figs.10-12 for F-F, F-S, S-S boundary conditions, respectively. For the forced

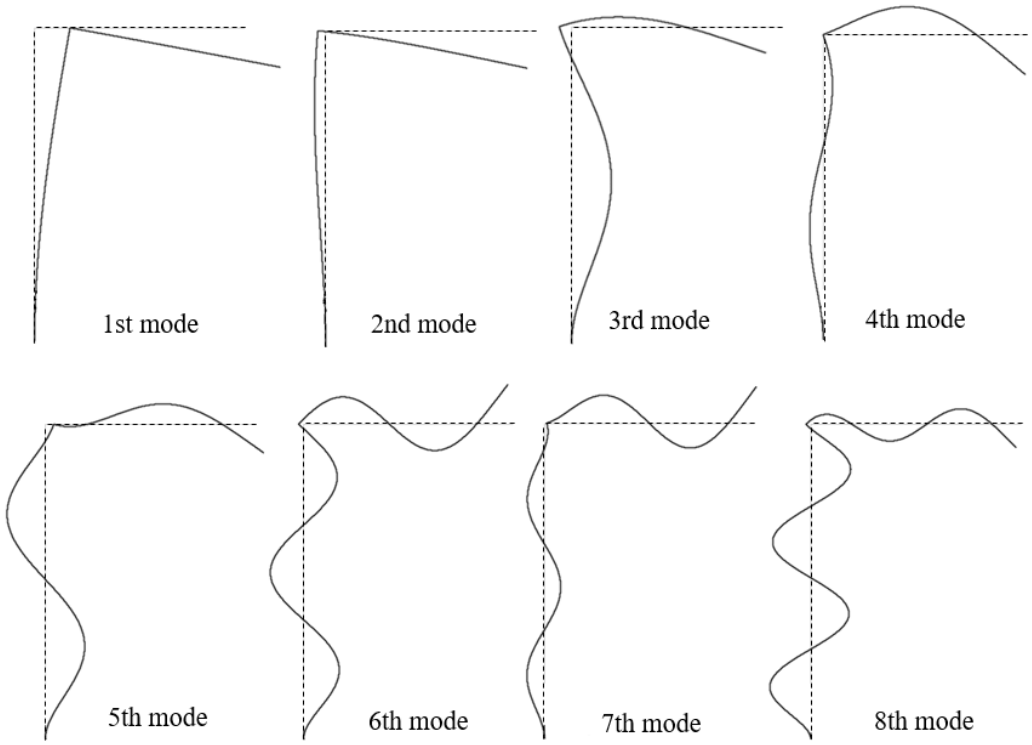

Fig. 6. First eight mode shapes of intact L-type frame model

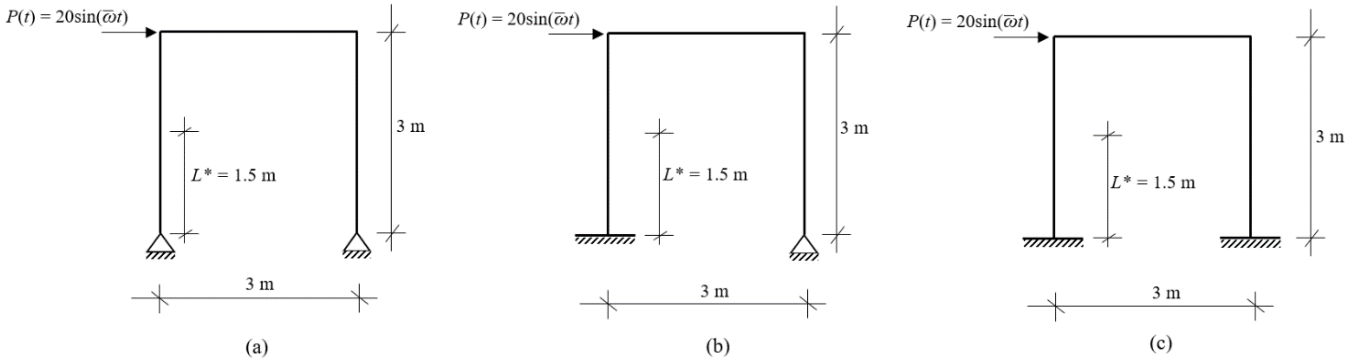

Fig. 7. a) Cracked single-bay single-story frame with S-S boundary condition, b) Cracked single-bay single-story frame with F-S boundary condition and c) Cracked single-bay single-story frame with F-F boundary condition

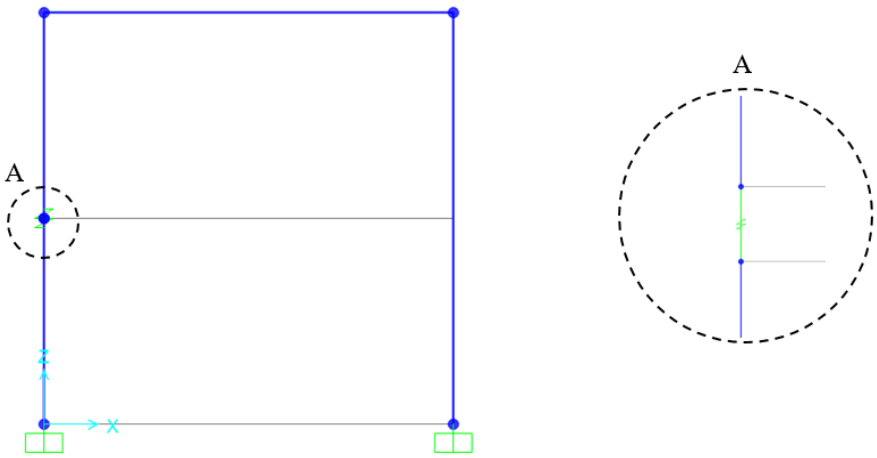

Fig. 8. Cracked single-bay single-story frame with F-F boundary condition in SAP2000

Table 3 First three natural frequencies of intact single-bay single-story frames

		Natural frequency (rads^{-1})			
Boundary condition	Mode	EBT	TBT	SVSDT	FEM
S-S	1st	40.5626	40.2720	40.3482	40.3010
	2nd	323.6715	316.3500	316.5611	317.8797
	3rd	436.7721	421.9356	423.9112	424.0312
F-S	1st	65.2848	64.4128	64.6662	64.4365
	2nd	354.8976	345.4844	346.0222	347.2470
	3rd	501.7379	479.7303	482.6143	482.5067
F-F	1st	85.7325	84.3439	84.7564	84.3762
	2nd	414.6869	400.2214	401.1641	402.6845
	3rd	610.5192	576.7871	583.3769	579.7040

Table 4 First three natural frequencies of cracked single-bay single-story frame with S-S boundary condition

		Natural frequency (rads^{-1})			
α	Mode	EBT	TBT	SVSDT	FEM
0.125	1st	40.4788	40.1491	39.3392	40.1776
	2nd	322.5565	314.7689	305.0638	316.6735
	3rd	435.2167	419.7936	415.2200	422.3997
0.25	1st	40.2356	39.7968	39.1476	39.8238
	2nd	319.2837	310.1520	300.9817	312.0609
	3rd	431.0190	414.2640	412.1882	416.8241
0.50	1st	39.0779	38.1951	38.2204	38.2161
	2nd	303.4642	289.0497	282.1197	290.9828
	3rd	416.3331	397.8700	401.8798	400.2923

Table 5 First three natural frequencies of cracked single-bay single-story frame with F-S boundary condition

		Natural frequency (rads^{-1})			
α	Mode	EBT	TBT	SVSDT	FEM
0.125	1st	65.2839	64.4113	62.0839	64.4353
	2nd	354.6652	345.1595	347.7092	347.0237
	3rd	500.9686	478.7329	477.9304	481.7685
0.25	1st	65.2813	64.4073	62.0700	64.4316
	2nd	353.9818	344.2082	346.7970	346.0709
	3rd	498.6318	475.6682	474.6666	478.7114
0.50	1st	65.2697	64.3905	62.0079	64.4162
	2nd	350.5454	339.5510	342.1405	341.4214
	3rd	485.7417	459.0299	458.9956	462.1461

vibration analysis of numerical case study, the harmonic response curves of intact and cracked frames are plotted according to a point dynamic load $P(t)$. The harmonic response curves represent a logarithmic scaled response of a node versus forcing frequency and TMM formulations provide response of boundaries. Thus, an appropriate response of supports of frame model should be chosen to plot harmonic responses. In this study, for S-S boundary condition, the harmonic response curves are plotted using the shear force response (Q_0) at the left hand side support.

Table 6 First three natural frequencies of cracked single-bay single-story frame with F-F boundary condition

		Natural frequency (rads^{-1})			
α	Mode	EBT	TBT	SVSDT	FEM
0.125	1st	85.0978	84.3438	83.2402	84.3760
	2nd	413.5565	399.3704	401.1067	402.0711
	3rd	596.9846	573.4145	573.9224	577.3091
0.25	1st	85.0951	84.3437	83.2370	84.3759
	2nd	410.6920	396.8705	398.5669	399.5559
	3rd	589.8685	562.7048	567.6429	566.7458
0.50	1st	85.0832	84.3435	83.2224	84.3758
	2nd	396.8325	384.7355	386.2111	387.3831
	3rd	562.0414	524.0146	542.0142	528.0200

The bending moment response (M_0) of left hand side support is used to obtain harmonic responses of frames having F-S and F-F boundary conditions. For the frame with S-S boundary condition, the harmonic response curves are presented in Figs.13-14 using SVSDT and TBT, respectively. Similarly, Figs. 15-16 represent harmonic response of intact and cracked frame model that has F-S boundary condition. The harmonic response curves of frame model having F-F boundary condition can be seen from Figs. 17-18 for SVSDT and TBT, respectively. By using EBT, the harmonic response curves of frame model with S-S boundary condition is presented in Fig.19. The harmonic response curves for the single-bay single-story frame model using EBT with F-S and F-F boundary conditions are presented in Figs.20-21, respectively.

From Figs. 13-21, the natural frequencies of intact and cracked frame models can be detected as resonant frequencies represented by peaks of harmonic response curves. It is observed from Figs. 13-21 that peaks of harmonic responses shift negatively by increasing crack ratio for all general boundary conditions and for EBT, SVSDT and TBT. For comparison purposes, harmonic response curves of intact single-bay single-story frames using EBT, TBT and SVSDT are presented in Figs. 22-24 for S-S, F-S and F-F boundary conditions, respectively. By using EBT, TBT and SVSDT comparatively, Figs. 25-27 are plotted for harmonic responses of cracked single-bay single-story frames for S-S, F-S and F-F boundary conditions, respectively.

The harmonic response curves allow very fast detection of natural frequencies as there is no need to use any root finding algorithm unlike standard analytical based solutions. It should be noted that elapsed time for calculating natural frequencies of single-bay single-story frame model using FEM is 4 seconds for all intact and cracked cases. The CPU usage times of MATLAB for calculating harmonic responses are presented in Table 8. According to Table 8, the proposed approach is significantly faster than FEM for calculation of natural frequencies of single-bay single-story frame. Table 8 shows that harmonic responses of EBT can be obtained slightly faster when compared to TBT and SVSDT. Although, there is no significant difference between CPU usage time of TBT and SVSDT.

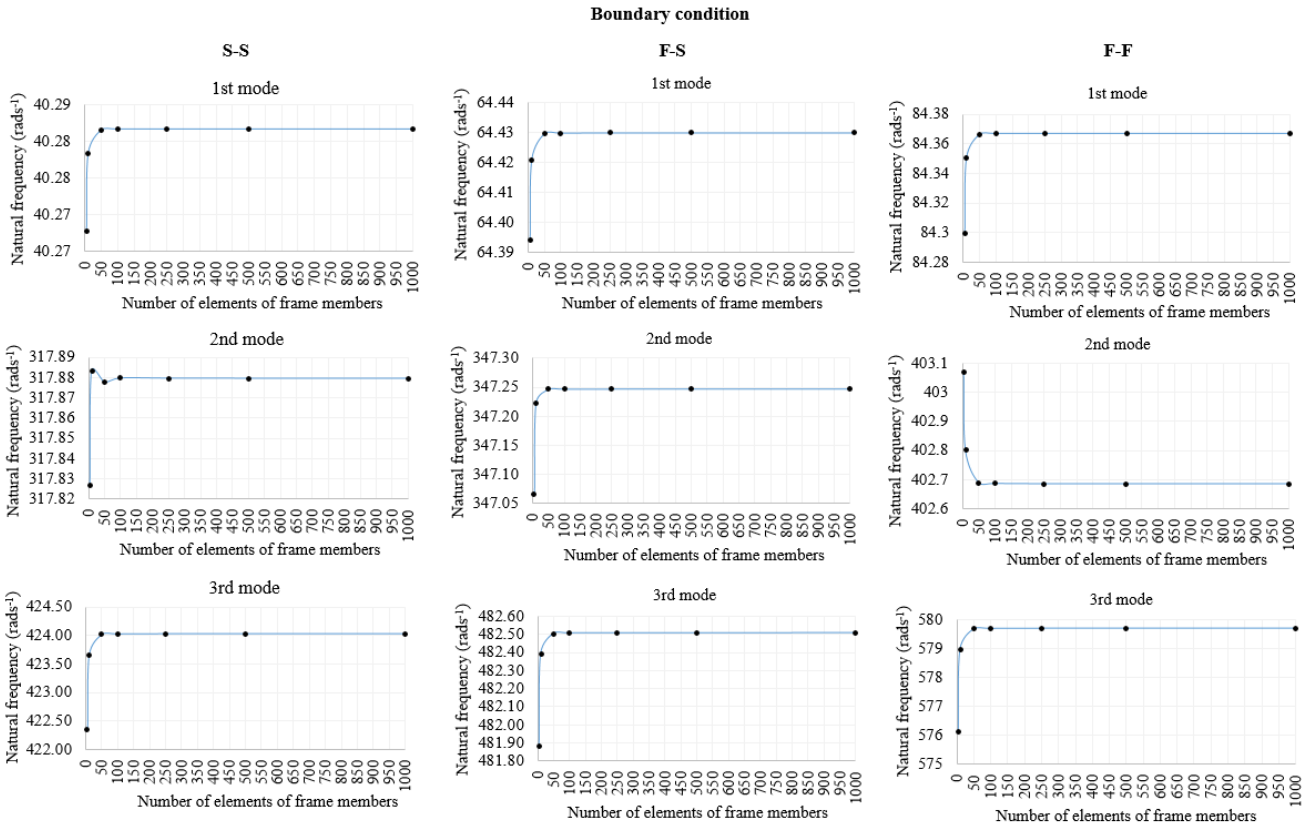

Fig. 9 FEM convergence for intact single-bay single story frame model

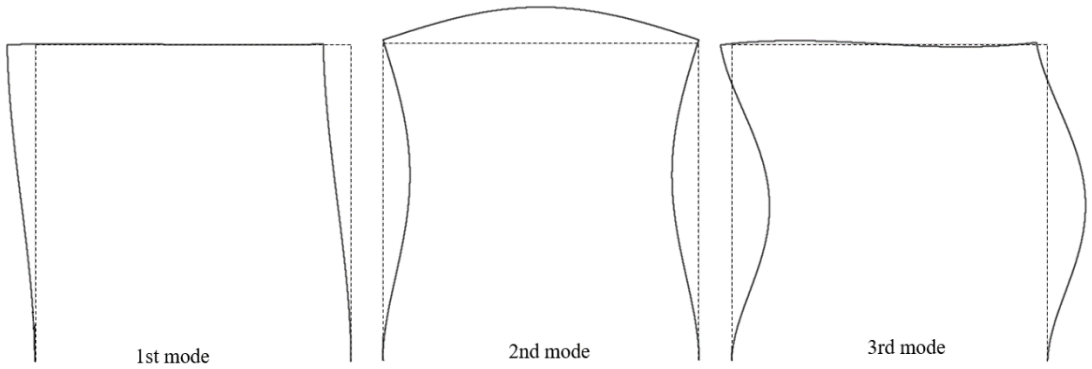

Fig. 10 First three mode shapes of intact single-bay single-story frame with F-F boundary conditions

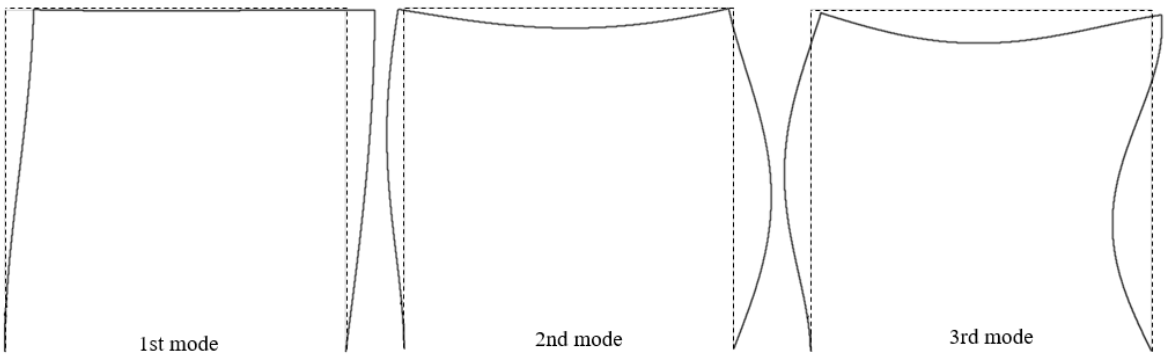

Fig. 11 First three mode shapes of intact single-bay single-story frame with F-S boundary conditions

Table 7 The relative errors between proposed approach and FEM for intact and cracked frames

Relative error (%)													
		Intact			α = 0.125			α = 0.25			α = 0.50		
Boundary condition	Mode	EBT	TBT	SVSDT	EBT	TBT	SVSDT	EBT	TBT	SVSDT	EBT	TBT	SVSDT
S-S	1st	0.65	0.07	0.12	0.75	0.07	2.09	1.03	0.07	1.70	2.26	0.05	0.01
	2nd	1.82	0.48	0.41	1.86	0.60	3.67	2.31	0.61	3.55	4.29	0.66	3.05
	3rd	3.00	0.49	0.03	3.03	0.62	1.70	3.41	0.61	1.11	4.01	0.61	0.40
F-S	1st	1.32	0.04	0.36	1.32	0.04	3.65	1.32	0.04	3.67	1.33	0.04	3.74
	2nd	2.20	0.51	0.35	2.20	0.54	0.20	2.29	0.54	0.21	2.67	0.55	0.21
	3rd	3.99	0.58	0.02	3.99	0.63	0.80	4.16	0.64	0.84	5.11	0.67	0.68
F-F	1st	1.61	0.04	0.45	0.86	0.00	1.35	0.33	0.04	1.35	0.84	0.00	1.37
	2nd	2.98	0.61	0.38	2.86	0.00	0.24	2.79	0.67	0.25	2.44	0.00	0.30
	3rd	5.32	0.50	0.63	3.41	0.00	0.59	4.08	0.71	0.16	6.44	0.00	2.65

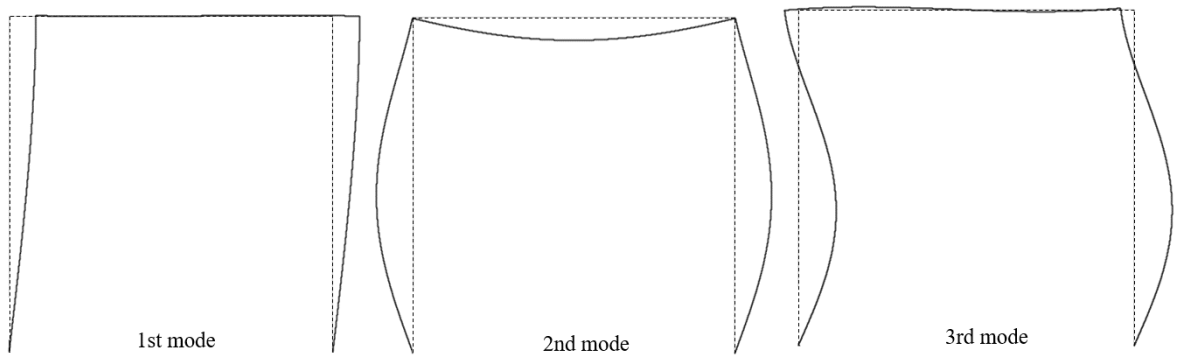

Fig. 12 First three mode shapes of intact single-bay single-story frame with S-S boundary conditions

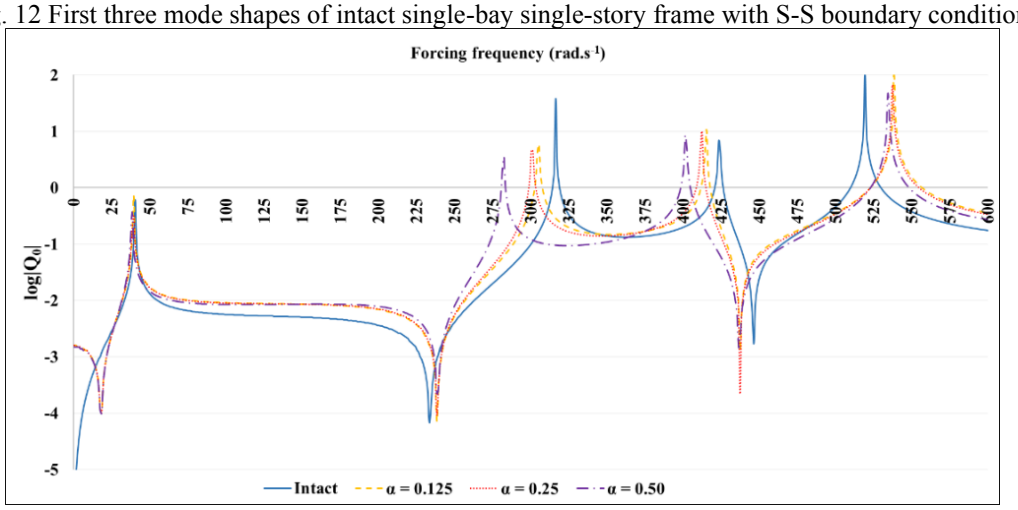

Fig. 13 Harmonic response curve of frame model with S-S boundary condition using SVSDT

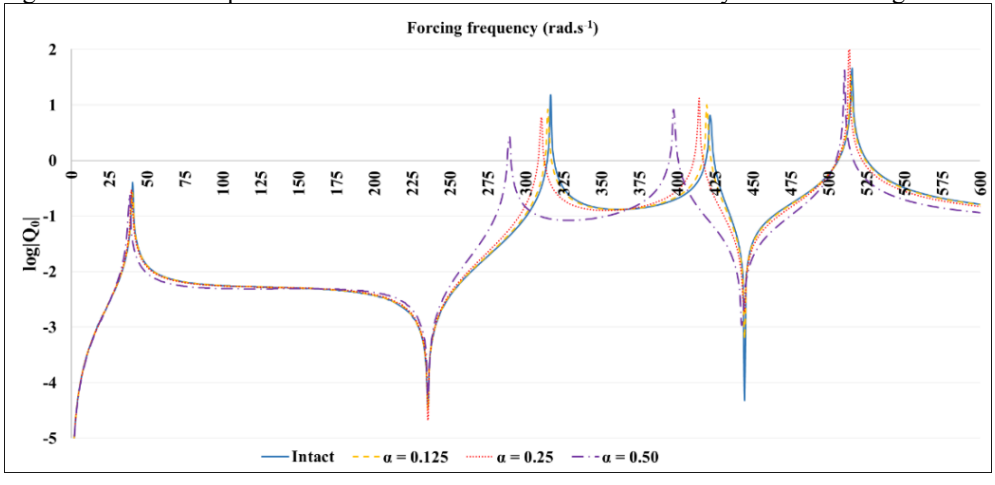

Fig. 14 Harmonic response curve of frame model with S-S boundary condition using TBT

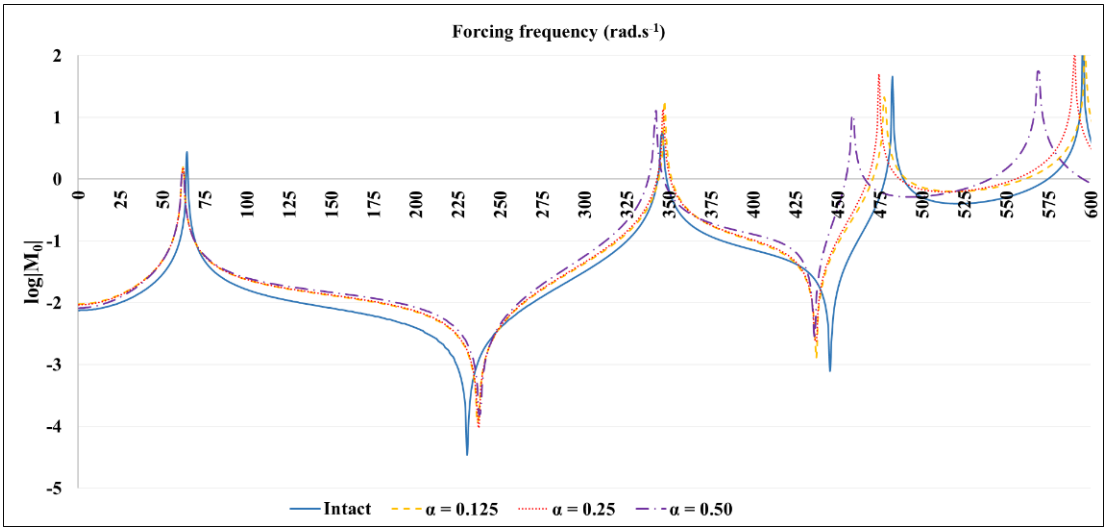

Fig. 15 Harmonic response curve of frame model with F-S boundary condition using SVSDT

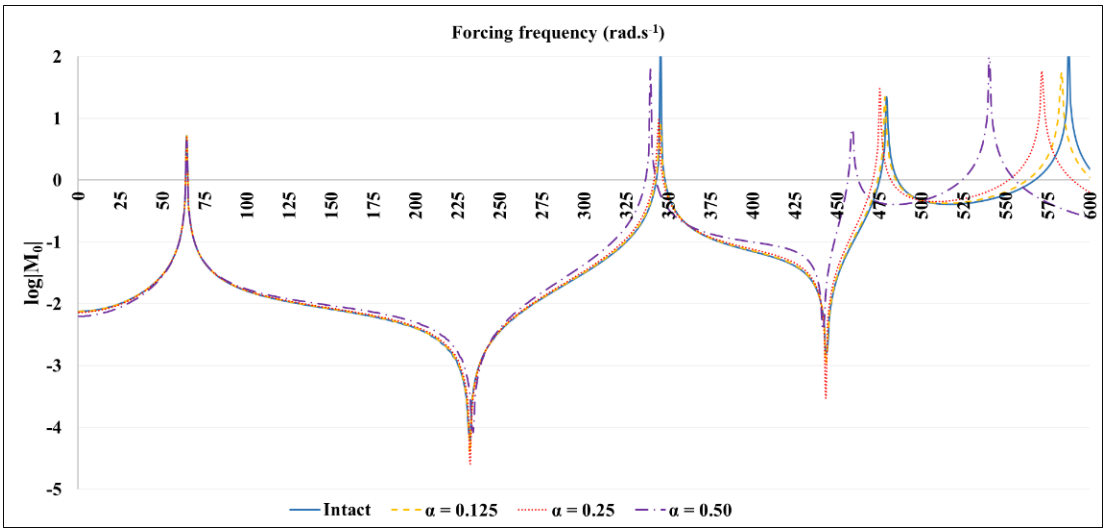

Fig. 16 Harmonic response curve of frame model with F-S boundary condition using TBT

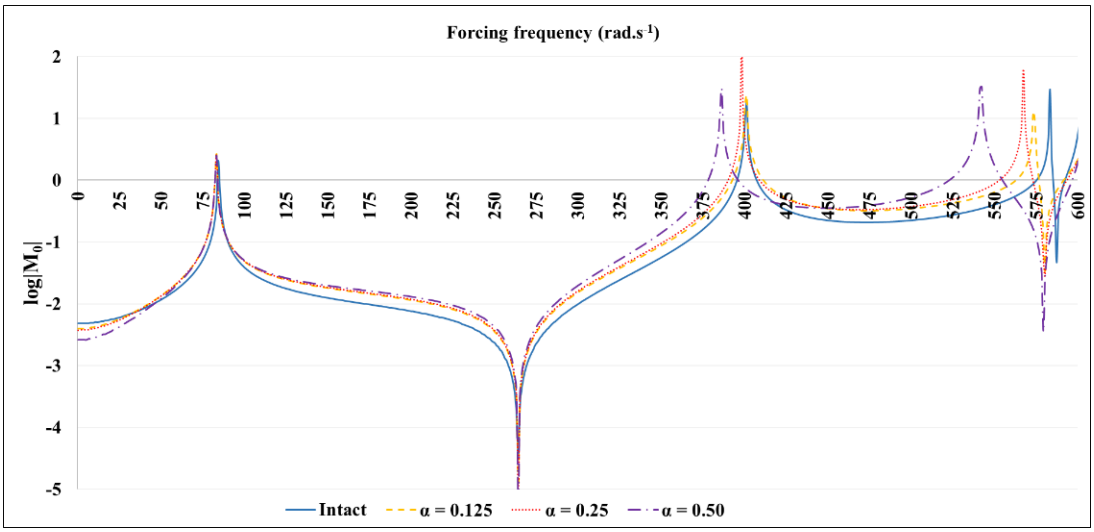

Fig. 17 Harmonic response curve of frame model with F-F boundary condition using SVSDT

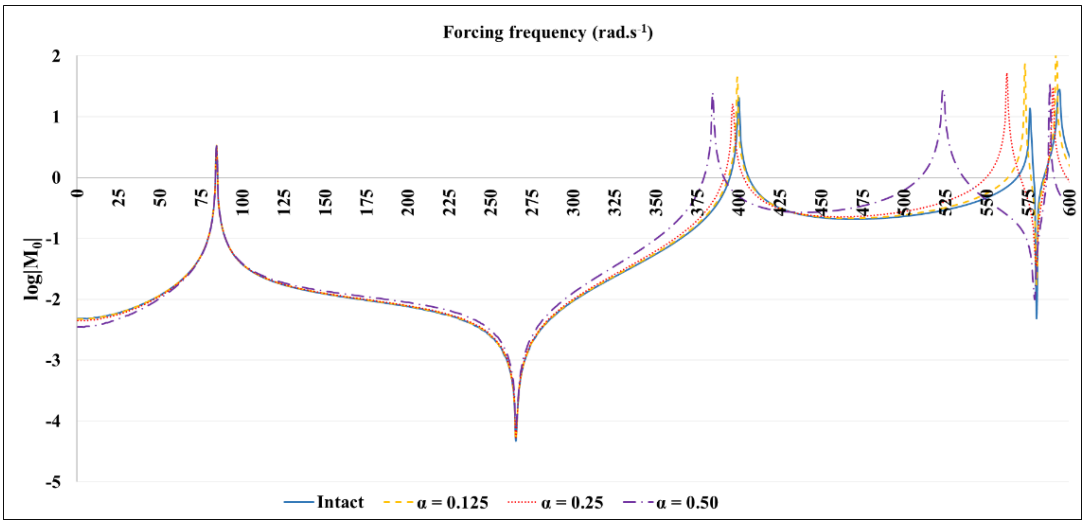

Fig. 18. Harmonic response curve of frame model with F-F boundary condition using TBT

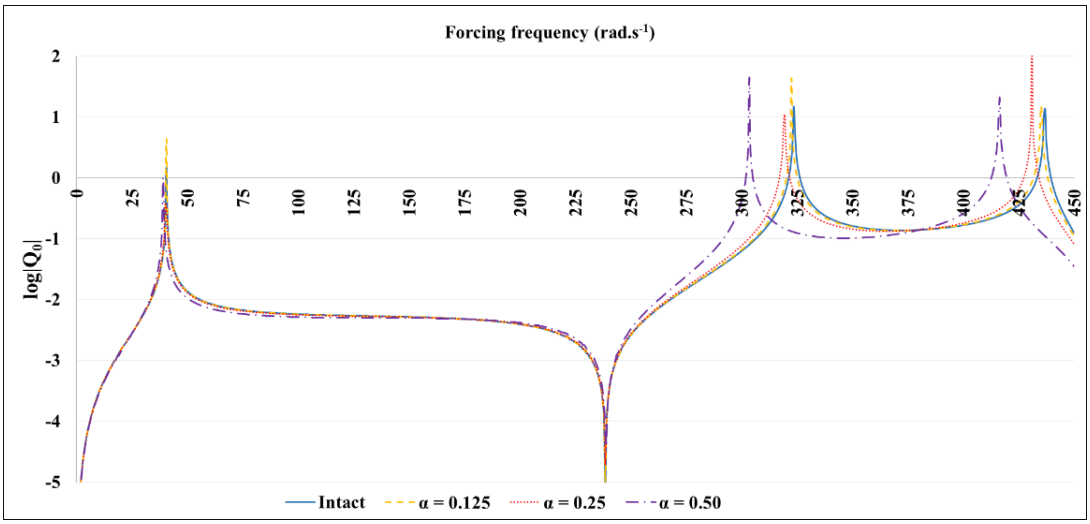

Fig. 19. Harmonic response curve of frame model with S-S boundary condition using EBT

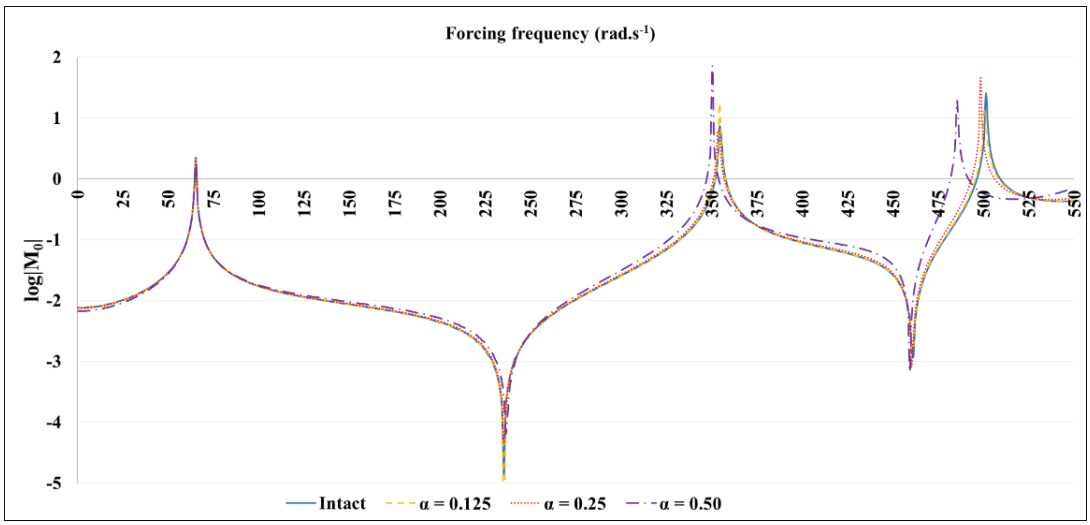

Fig. 20 Harmonic response curve of frame model with F-S boundary condition using EBT

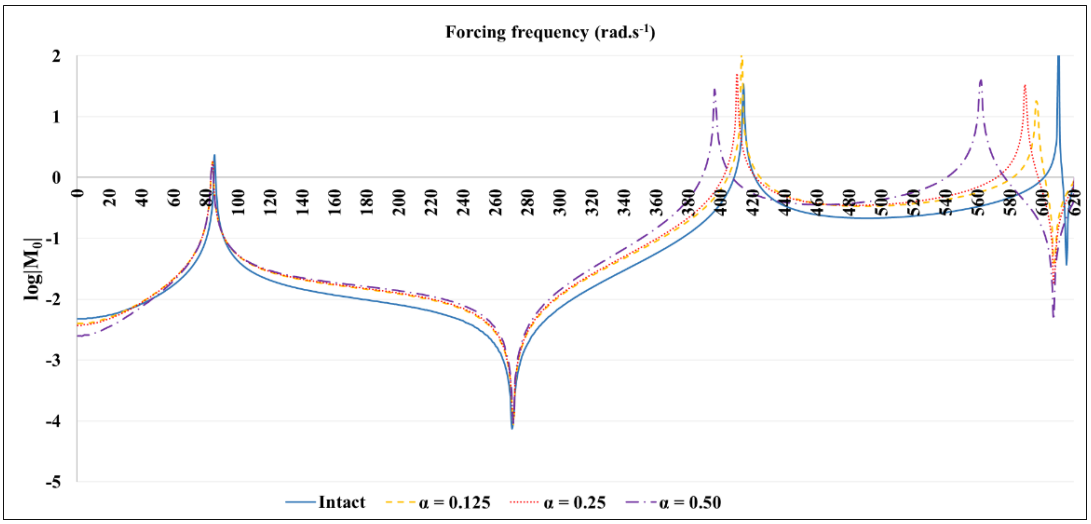

Fig. 21. Harmonic response curve of frame model with F-F boundary condition using EBT

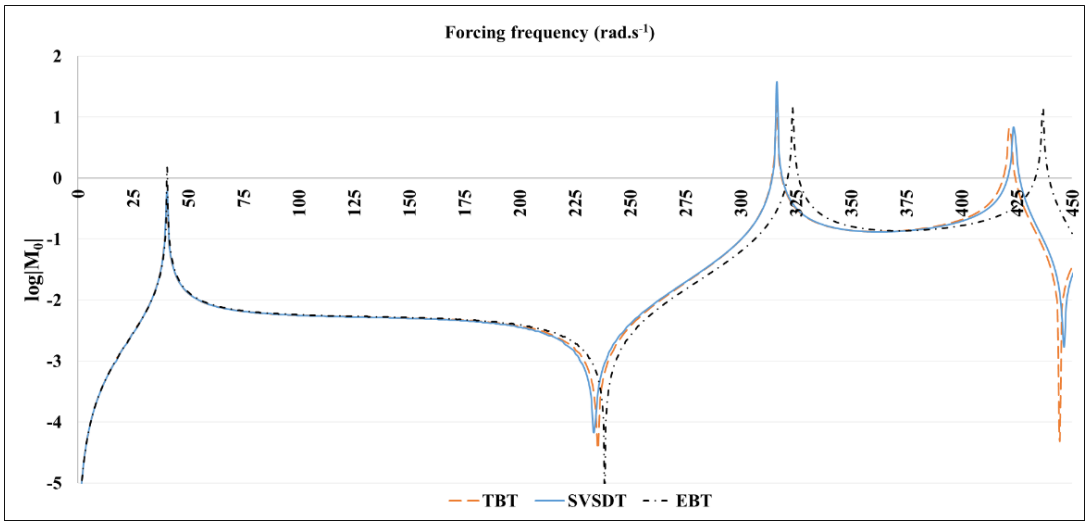

Fig. 22 Harmonic response curve of intact frame model with S-S boundary condition using EBT, TBT and SVSDT

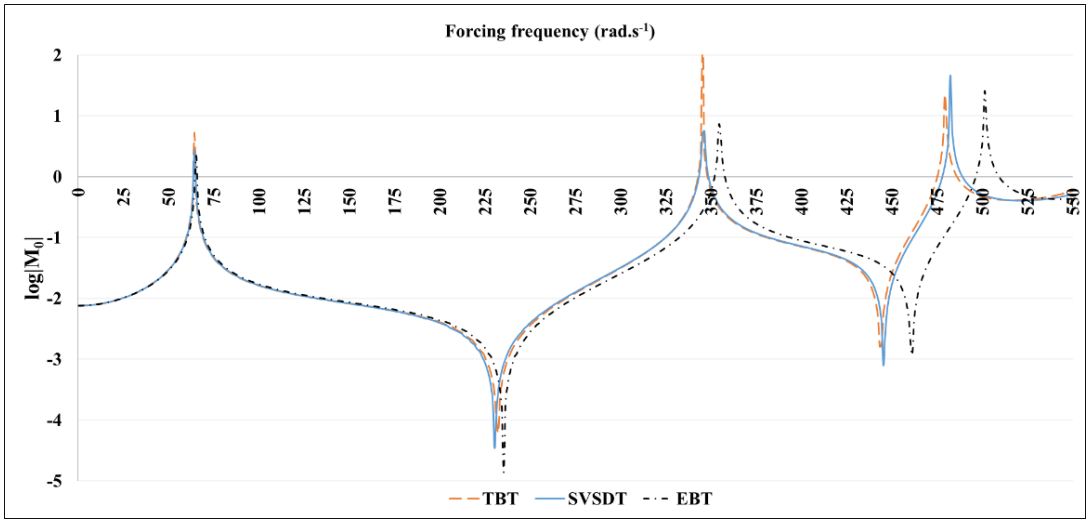

Fig. 23 Harmonic response curve of intact frame model with F-S boundary condition using EBT, TBT and SVSDT

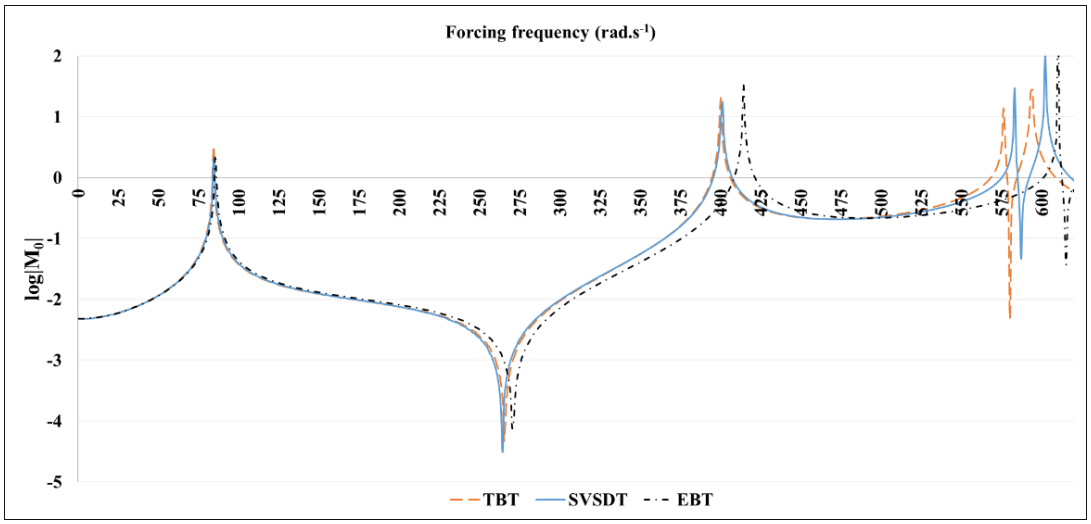

Fig. 24 Harmonic response curve of intact frame model with F-F boundary condition using EBT, TBT and SVSDT

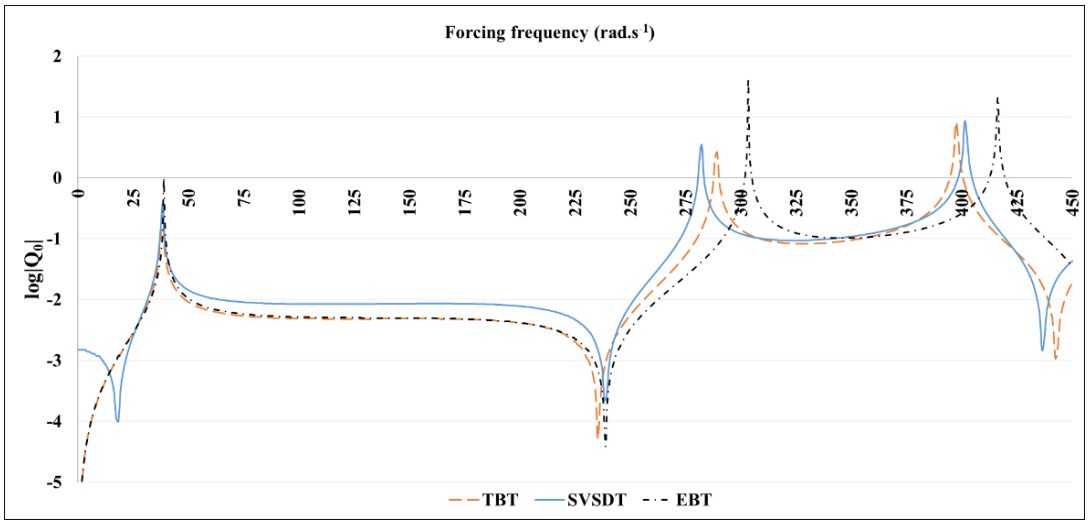

Fig. 25 Harmonic response curve of cracked frame model with S-S boundary condition using EBT, TBT and SVSDT (α=0.50)

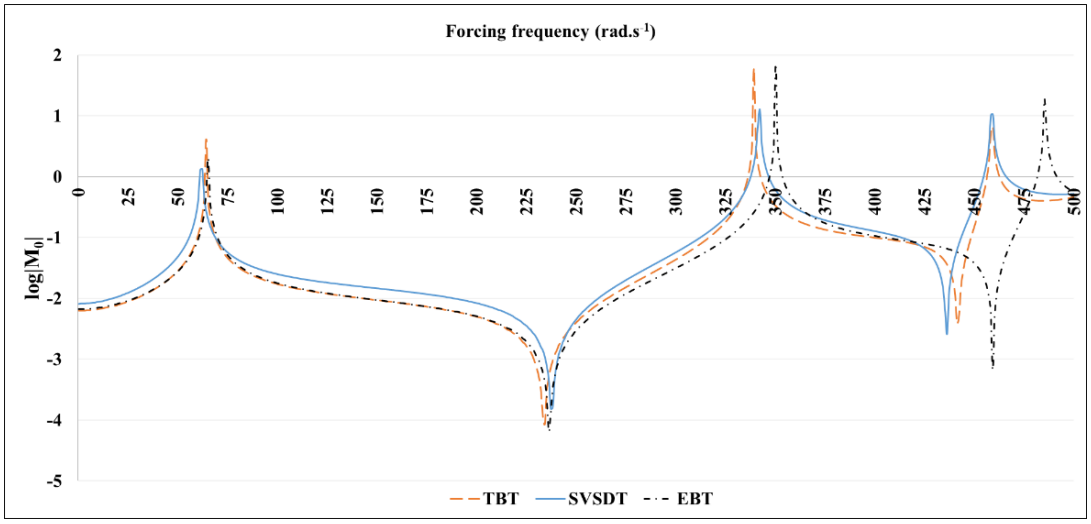

Fig. 26 Harmonic response curve of cracked frame model with F-S boundary condition using EBT, TBT and SVSDT (α=0.50)

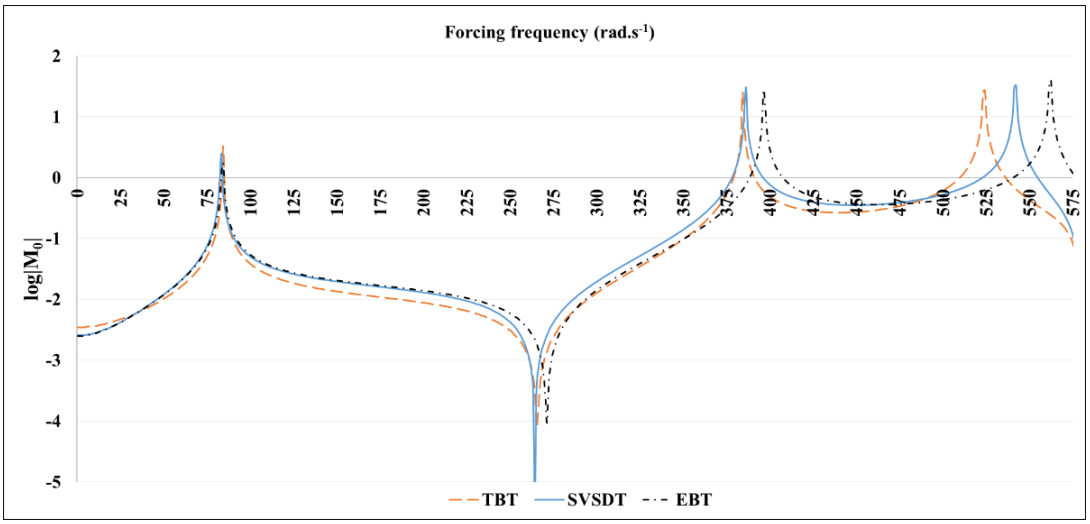

Fig. 27 Harmonic response curve of cracked frame model with F-F boundary condition using EBT, TBT and SVSDT (α=0.50)

Table 8 CPU usage time for calculation of harmonic responses using EBT, TBT and SVSDT

	CPU usage time (sec)					
	Intact frame			Cracked frame		
Boundary condition	EBT	TBT	SVSDT	EBT	TBT	SVSDT
S-S	0.439	0.552	0.560	0.447	0.580	0.583
F-S	0.332	0.567	0.556	0.314	0.579	0.565
F-F	0.450	0.597	0.556	0.334	0.579	0.576

6. Conclusions

In this study, the forward problem of calculation of the natural frequencies of cracked frames is exactly solved by using the SVSDT, which considers a parabolic shear stress distribution along cross-section of frame members. The transfer matrix formulations are derived and applied to free vibrations of cracked frame structures. Moreover, the harmonic response curves of cracked frames, which allow to detect natural frequencies without using any root-finding algorithm, are plotted via transfer matrix formulations according to a dynamic point load. It is proved that the TMM can be used as a powerful tool for harmonic response analysis of frame structures. The dimension of global transfer matrix of whole vibrating system is irrespective of the number of cracks or any other concentrated attachments on frame members. Therefore, the computer programs prepared for free and forced vibration analysis of cracked frames using TMM are working fast for both SVSDT, TBT, as well as EBT. It is predictable that the significant difference between computation times of proposed approach and FEM would become larger for more complicated structures like multi-bay multi-story frames or 3-D frames as a result of using thousands of finite elements for accurate results.

The TMM would be very effective for harmonic response and free vibration analysis of multiple-cracked frame structures as the method is based on chain-multiplication of member global transfer matrices and jump matrices arised from cracks. Unlike other analytical based methods that are effective for on frame vibrations such as dynamic stiffness approach, the dimension of overall global transfer matrix of whole vibrating system is not affected by number of members as well as number of cracks. Therefore, computation time of TMM for multiple-cracked frames would remain very well when compared to other exact methods. The formulations of SVSDT are very straightforward when compared to TBT. Moreover, the SVSDT provides EBT results as a special case by ignoring shear related terms from governing equation of motion. This advantage of SVSDT would be used effectively in future studies on cracked beam-assembly structures considering and ignoring shear deformation and rotational inertia effects via the same formulations.

References

MATLAB (2014), MATLAB R2014b, The MathWorks Inc., MI, U.S.A.

SAP2000 (2013), SAP2000 V 16.0.0, Integrated Solution for Structural Analysis & Design, Computers & Structures Inc., U.S.A.

Anagnostides, G. (1986), "Frame response to a harmonic excitation, taking into account the effects of shear deformation and rotary inertia", *Comput. Struct.*, **24**(2), 295-304. https://doi.org/10.1016/0045-7949(86)90287-7.

Areias, P. and Rabczuk, T. (2013), "Finite strain fracture of plates and shells with configurational forces and edge rotations", *Int. J. Numer. Meth. Eng.*, **94**(12), 1099-1122. https://doi.org/10.1002/nme.4477.

Areias, P., Rabczuk, T. and Msekh, M.A. (2016), "Phase-field analysis of finite-strain plates and shells including element subdivision", *Comput. Method Appl. M.*, **312**, 322-350 https://doi.org/10.1016/j.cma.2016.01.020.

Attar, M. (2012), "A transfer matrix method for free vibration analysis and crack identification of stepped beams with multiple edge cracks and different boundary conditions", *Int. J. Mech. Sci.*, **57**(1), 19-33. https://doi.org/10.1016/j.ijmecsci.2012.01.010.

Attar, M., Karrech, A. and Regenauer-Lieb, K. (2014), "Free vibration analysis of a cracked shear deformable beam on a two-parameter elastic foundation using a lattice spring model", *J.*

Sound Vib., **333**(11), 2359-2377. https://doi.org/10.1016/j.jsv.2013.11.013

Barad, K.H., Sharma, D.S. and Vyas, V. (2013), "Crack Detection in Cantilever Beam by Frequency based Method", *Procedia Eng.*, **51**, 770-775. https://doi.org/10.1016/j.proeng.2013.01.110

Bickford, W.B. (1982), "Consistent higher order beam theory", *Developments in Theoretical and Applied Mechanics*, Springer, Germany.

Bozyigit, B. and Yesilce, Y. (2018), "Natural frequencies and harmonic responses of multi-story frames using single variable shear deformation theory", *Mech. Res. Commun.*, **92**, 28-36. https://doi.org/10.1016/j.mechrescom.2018.06.007

Brasiliano, A., Doz, G.N. and de Brito, J.L.V. (2004), "Damage identification in continuous beams and frame structures using the Residual Error Method in the Movement Equation", *Nucl. Eng. Des.*, **227**(1), 1-17. https://doi.org/10.1016/j.nucengdes.2003.07.006

Caddemi, S. and Caliò, I. (2013), "The exact explicit dynamic stiffness matrix of multi-cracked Euler–Bernoulli beam and applications to damaged frame structures", *J. Sound Vib.*, **332**(12), 3049-3063. https://doi.org/10.1016/j.jsv.2013.01.003

Carden, E.P. and Fanning, P. (2004), "Vibration Based Condition Monitoring: A Review", *Struct. Health Monit.*, **3**(4), 355-377. https://doi.org/10.1177/1475921704047500.

Chondros, T.G., Dimarogonas, A.D. and Yao, J. (1998), "A CONTINUOUS CRACKED BEAM VIBRATION THEORY", *J. Sound Vib.*, **215**(1), 17-34. https://doi.org/10.1006/jsvi.1998.1640.

Cunedioglu, Y (2015), "Free vibration analysis of edge cracked symmetric functionally graded sandwich beams", *Struct. Eng. Mech.*,, **56**(6), 1003-1020.

Dastjerdi, S. and Abbasi, M. (2019), "A vibration analysis of a cracked micro-cantilever in an atomic force microscope by using transfer matrix method", *Ultramicroscopy*, **196**, 33-39 https://doi.org/10.1016/j.ultramic.2018.09.014

Elshamy, M., Crosby, W.A. and Elhadary, M. (2018), "Crack detection of cantilever beam by natural frequency tracking using experimental and finite element analysis", *Alexandria Eng. J.*, **57**(4), 3755-3766. https://doi.org/10.1016/j.aej.2018.10.002.

Gillich, G-R, Furdui, H, Abdel Wahab, M and Korka, Z-I (2019), "A robust damage detection method based on multi-modal analysis in variable temperature conditions", *Mech. Syst. Signal Processing*., **115**, 361-379.

Greco, A. and Pau, A. (2012), "Damage identification in Euler frames", *Comput. Struct.*, **92-93**, 328-336. https://doi.org/10.1016/j.compstruc.2011.10.007.

Han, S.M., Benaroya, H. and Wei, T. (1999), "DYNAMICS OF TRANSVERSELY VIBRATING BEAMS USING FOUR ENGINEERING THEORIES", *J. Sound Vib.*, **225**(5), 935-988. https://doi.org/10.1006/jsvi.1999.2257.

Heyliger, P.R. and Reddy, J.N. (1988), "A higher order beam finite element for bending and vibration problems", *J. Sound Vib.*, **126**(2), 309-326. https://doi.org/10.1016/0022-460X(88)90244-1.

Khatir, S., Dekemele, K., Loccufier, M., Khatir, T. and Abdel Wahab, M. (2018), "Crack identification method in beam-like structures using changes in experimentally measured frequencies and Particle Swarm Optimization", *Comptes Rendus Mécanique*, **346**(2), 110-120. https://doi.org/10.1016/j.crme.2017.11.008.

Khatir, S. and Abdel Wahab, M. (2019), "Fast simulations for solving fracture mechanics inverse problems using POD-RBF XIGA and Jaya algorithm", *Eng. Fracture Mech.*, **205**, 285-300. https://doi.org/10.1016/j.engfracmech.2018.09.032.

Khatir, S., Abdel Wahab, M., Boutchicha, D. and Khatir, T. (2019), "Structural health monitoring using modal strain energy damage indicator coupled with teaching-learning-based optimization algorithm and isogoemetric analysis", *J. Sound Vib.*, **448**, 230-246. https://doi.org/10.1016/j.jsv.2019.02.017.

Khiem, N.T. and Lien, T.V. (2001), "A simplified method for natural frequency analysis of a multiple cracked beam", *J. Sound Vib.*, **245**(4), 737-751. https://doi.org/10.1006/jsvi.2001.3585

Khiem, N.T. and Lien, T.V. (2004), "Multi-crack detection for beam by the natural frequencies", *J. Sound Vib.*, **273**(1), 175-184. https://doi.org/10.1016/S0022-460X(03)00424-3

Khiem, N.T. and Toan, L.K. (2014), "A novel method for crack detection in beam-like structures by measurements of natural frequencies", *J. Sound Vib.*, **333**(18), 4084-4103. https://doi.org/10.1016/j.jsv.2014.04.031.

Khnaijar, A. and Benamar, R. (2017), "A new model for beam crack detection and localization using a discrete model", *Eng. Struct.*, **150**, 221-230. https://doi.org/10.1016/j.engstruct.2017.07.034.

Kim, K., Kim, S., Sok, K., Pak, C. and Han, K. (2018), "A modeling method for vibration analysis of cracked beam with arbitrary boundary condition", *J. Ocean Eng. Sci.*, **3**(4), 367-381. https://doi.org/10.1016/j.joes.2018.11.003.

Kindova-Petrova, D. (2014), "Vibration-Based Methods for Detecting A Crack In A Simply Supported Beam", *J. Theor. Appl. Mech.*, **44**(4), 69-82. https://doi.org/10.2478/jtam-2014-0023.

Labib, A., Kennedy, D. and Featherston, C. (2014), "Free vibration analysis of beams and frames with multiple cracks for damage detection", *J. Sound Vib.*, **333**(20), 4991-5003. https://doi.org/10.1016/j.jsv.2014.05.015.

Lee, J.W. and Lee, J.Y. (2017), "In-plane bending vibration analysis of a rotating beam with multiple edge cracks by using the transfer matrix method", *Meccanica*, **52**(4), 1143-1157. 10.1007/s11012-016-0449-4.

Lee, J.W. and Lee, J.Y. (2017), "A transfer matrix method capable of determining the exact solutions of a twisted Bernoulli–Euler beam with multiple edge cracks", *Appl. Math. Model.*, **41**, 474-493 https://doi.org/10.1016/j.apm.2016.09.013.

Levinson, M. (1981), "A new rectangular beam theory", *J. Sound Vib.*, **74**(1), 81-87. https://doi.org/10.1016/0022-460X(81)90493-4.

Loya, J.A., Rubio, L. and Fernández-Sáez, J. (2006), "Natural frequencies for bending vibrations of Timoshenko cracked beams", *J. Sound Vib.*, **290**(3), 640-653. https://doi.org/10.1016/j.jsv.2005.04.005.

Moezi, S.A., Zakeri, E. and Zare, A. (2018), "Structural single and multiple crack detection in cantilever beams using a hybrid Cuckoo-Nelder-Mead optimization method", *Mech. Syst. Signal Pr.*, **99**, 805-831. https://doi.org/10.1016/j.ymssp.2017.07.013.

Nguyen-Thanh, N., Valizadeh, N., Nguyen, M.N., Nguyen-Xuan, H., Zhuang, X., Areias, P., Zi, G., Bazilevs, Y., De Lorenzis, L. and Rabczuk, T. (2015), "An extended isogeometric thin shell analysis based on Kirchhoff–Love theory", *Comput. Method Appl. M.*, **284**, 265-291. https://doi.org/10.1016/j.cma.2014.08.025.

Nguyen, H.X., Nguyen, T.N., Abdel-Wahab, M., Bordas, S.P.A., Nguyen-Xuan, H. and Vo, T.P. (2017), "A refined quasi-3D isogeometric analysis for functionally graded microplates based on the modified couple stress theory", *Comput. Method Appl. M.*, **313**, 904-940. https://doi.org/10.1016/j.cma.2016.10.002.

Nguyen, N.-T., Hui, D., Lee, J. and Nguyen-Xuan, H. (2015), "An efficient computational approach for size-dependent analysis of functionally graded nanoplates", *Comput. Method Appl. M.*, **297**, 191-218. https://doi.org/10.1016/j.cma.2015.07.021.

Nguyen, T.N., Ngo, T.D. and Nguyen-Xuan, H. (2017), "A novel three-variable shear deformation plate formulation: Theory and Isogeometric implementation", *Comput. Method Appl. M.*, **326**, 376-401. https://doi.org/10.1016/j.cma.2017.07.024.

Nguyen, T.N., Thai, C.H. and Nguyen-Xuan, H. (2016), "On the

general framework of high order shear deformation theories for laminated composite plate structures: A novel unified approach", *Int. J. Mech. Sci.*, **110**, 242-255. https://doi.org/10.1016/j.ijmecsci.2016.01.012.

Nikolakopoulos, P.G., Katsareas, D.E. and Papadopoulos, C.A. (1997), "Crack identification in frame structures", *Comput. Struct.*, **64**(1), 389-406. https://doi.org/10.1016/S0045-7949(96)00120-4.

Ntakpe, J.L., Gillich, G.R., Muntean, F., Praisach, Z.I. and Lorenz, P. (2014), "Vibration-Based Crack Detection in L-Frames", *Appl. Mech. Mater.*, **658**, 261-268 10.4028/www.scientific.net/AMM.658.261.

Ostachowicz, W.M. and Krawczuk, M. (1991), "Analysis of the effect of cracks on the natural frequencies of a cantilever beam", *J. Sound Vib.*, **150**(2), 191-201. https://doi.org/10.1016/0022-460X(91)90615-Q.

Rabczuk, T., Areias, P.M.A. and Belytschko, T. (2007), "A meshfree thin shell method for non-linear dynamic fracture", *Int. J. Numer. Meth. Eng.*, **72**(5), 524-548. https://doi.org/10.1002/nme.2013.

Rabczuk, T., Gracie, R., Song, J.-H. and Belytschko, T. (2010), "Immersed particle method for fluid–structure interaction", *Int. J. Numer. Meth. Eng.*, **81**(1), 48-71. https://doi.org/10.1002/nme.2670.

Rao, S.S. (1995), *Mechanical Vibrations*, Edison-Wesley Publishing Company, U.S.A.

Satpute, D., Baviskar, P., Gandhi, P., Chavanke, M. and Aher, T. (2017), "Crack Detection in Cantilever Shaft Beam Using Natural Frequency", *Mater. Today-Proc.*, **4**(2), 1366-1374. https://doi.org/10.1016/j.matpr.2017.01.158.

Shahverdi, H., Navardi, MM (2017), "Free vibration analysis of cracked thin plates using generalized differential quadrature element method", *Struct. Eng. Mech.*, **62**(3), 345-355.

Shimpi, R.P., Shetty, R.A. and Guha, A. (2017), "A simple single variable shear deformation theory for a rectangular beam", *P. I. Mech. Eng. C-J. Mec.*, **231**(24), 4576-4591. https://doi.org/10.1177/0954406216670682.

Tan, G.J., Shan, J.H., Wu, C.L. and Wang, W.S. (2017), "Free vibration analysis of cracked Timoshenko beams carrying spring-mass systems", *Struct. Eng. Mech.,* **63**(4), 551-565.

Thalapil, J. and Maiti, S.K. (2014), "Detection of longitudinal cracks in long and short beams using changes in natural frequencies", *Int. J. Mech. Sci.*, **83**, 38-47. https://doi.org/10.1016/j.ijmecsci.2014.03.022.

Tiachacht, S., Bouazzouni, A., Khatir, S., Abdel Wahab, M., Behtani, A. and Capozucca, R. (2018), "Damage assessment in structures using combination of a modified Cornwell indicator and genetic algorithm", *Eng. Struct.*, **177**, 421-430.

Umar, S., Bakhary, N. and Abidin, A.R.Z. (2018), "Response surface methodology for damage detection using frequency and mode shape", *Measurement*, **115**, 258-268. https://doi.org/10.1016/j.measurement.2017.10.047.

CC

Appendix

The governing equation of a motion of beam in free vibration according to EBT is presented in Eq.(A.1) (Barad *et al.* 2013).

$$EI\frac{\partial^4 y(x,t)}{\partial x^4}+\bar{m}\frac{\partial^2 y(x,t)}{\partial t^2}=0 \tag{A.1}$$

where $y(x,t)$ is transverse displacement function. Eq.(A.2) is obtained by applying separation of variables method with the assumption of $y(x,t) = y(x)e^{i\omega t}$.

$$\frac{d^4 y(z)}{dz^4}-\left(\frac{\bar{m}\omega^2 L^4}{EI}\right)y(z)=0 \tag{A.2}$$

Assuming the solution of Eq.(A.2) is in the following form:

$$y(z)=\{\bar{C}\}e^{irz} \tag{A.3}$$

By substituting Eq.(A.3) into Eq.(A.2), $y(z)$ and slope function $\frac{dy}{dz}$ are obtained as in Eqs.(A.4)-(A.5), respectively.

$$y(z)=(\bar{C}_1e^{ir_1z}+\bar{C}_2e^{ir_2z}+\bar{C}_3e^{ir_3z}+\bar{C}_4e^{ir_4z}) \tag{A.4}$$

$$\frac{dy}{dz}=(ir_1\bar{C}_1e^{ir_1z}+is_2\bar{C}_2e^{ir_2z}+is_3\bar{C}_3e^{ir_3z}+is_4\bar{C}_4e^{ir_4z}) \tag{A.5}$$

Bending moment function $M^E(z)$ and shear force function $Q^E(z)$ are defined as:

$$M^E(z)=\frac{EI}{L^2}(r_1^2\bar{C}_1e^{ir_1z}+r_2^2\bar{C}_2e^{ir_2z}+r_3^2\bar{C}_3e^{ir_3z}+r_4^2\bar{C}_4e^{ir_4z}) \tag{A.6}$$

$$Q^E(z)=\frac{EI}{L^3}(ir_1^3\bar{C}_1e^{ir_1z}+ir_2^3\bar{C}_2e^{ir_2z}+ir_3^3\bar{C}_3e^{ir_3z}+ir_4^3\bar{C}_4e^{ir_4z}) \tag{A.7}$$

The state vectors and transfer matrices of frame members according to EBT can be constructed without any difficulty using Eqs.(A.4)-(A.7) and Eqs.(17)-(18). The governing equation of a motion of a Timoshenko beam free vibration can be written as follows (Bozyigit and Yesilce 2018):

$$\frac{AG}{\bar{k}}\left(\frac{\partial^2 w(x,t)}{\partial x^2}-\frac{\partial\varphi(x,t)}{\partial x}\right)-\bar{m}\frac{\partial^2 w(x,t)}{\partial t^2}=0 \tag{A.8}$$

$$EI\frac{\partial\varphi^2(x,t)}{\partial x^2}-\frac{\bar{m}I}{A}\frac{\partial\varphi^2(x,t)}{\partial t^2}+\frac{AG}{\bar{k}}\left(\frac{\partial w(x,t)}{\partial x}-\varphi(x,t)\right)=0 \tag{A.9}$$

where $w(x,t)$ is transverse displacement function, $\varphi(x,t)$ is rotation function due to bending, $\bar{k}$ is shear correction factor and G is shear modulus.

The bending moment function $M^T(x,t)$ and the shear force function $Q^T(x,t)$ of the Timoshenko beam are written as:

$$M^T(x,t)=EI\frac{\partial\varphi(x,t)}{\partial x} \tag{A.10}$$

$$Q^T(x,t)=\frac{AG}{\bar{k}}\gamma(x,t)=\frac{AG}{\bar{k}}\left(\frac{\partial w(x,t)}{\partial x}-\varphi(x,t)\right) \tag{A.11}$$

Eqs.(A.12)-(A.13) are obtained by applying separation of variables method with the assumption of $w(x,t) = w(x)e^{i\omega t}$ and $\varphi(x,t) = \varphi(x)e^{i\omega t}$.

$$\left(\frac{AG}{\bar{k}L^2}\right)\frac{d^2w}{dz^2}-\left(\frac{AG}{L\bar{k}}\right)\frac{d\varphi}{dz}+\left(\bar{m}\omega^2\right)w(z)=0 \tag{A.12}$$

$$\frac{EI}{L^2}\frac{d^2\varphi}{dz^2}+\left(\frac{AG}{L\bar{k}}\right)\frac{dw}{dz}+\left(\frac{\bar{m}\omega^2 I}{A}-\frac{AG}{\bar{k}}\right)\varphi(z)=0 \tag{A.13}$$

It is assumed that the solution of $w(z)$ and $\varphi(z)$ are in the following forms:

$$w(z)=\{\bar{D}\}e^{ipz} \tag{A.14}$$

$$\varphi(z)=\{\bar{E}\}e^{ipz} \tag{A.15}$$

where p represents characteristic roots obtained from substituting Eqs.(A.14)-(A.15) into Eqs.(A.12)-(A.13). Substituting Eqs.(A.14) and (A.15) into Eqs.(A.12)-(A.13) results in

$$\left[\bar{m}\omega^2-\left(\frac{AG}{\bar{k}L^2}\right)p^2\right]\{\bar{D}\}-\left(\frac{AG}{L\bar{k}}ip\right)\{\bar{E}\}=0 \tag{A.16}$$

$$\left(\frac{AG}{L\bar{k}}ip\right)\{\bar{D}\}+\left(\frac{\bar{m}\omega^2 I}{A}-\frac{AG}{\bar{k}}-\frac{EI}{L^2}p^2\right)\{\bar{E}\}=0 \tag{A.17}$$

Eqs.(A.16)-(A.17) can be written in matrix form for the two unknown integration constant vectors as:

$$\begin{bmatrix}A_{11} & A_{12}\\ A_{21} & A_{22}\end{bmatrix}\begin{Bmatrix}\{\bar{D}\}\\ \{\bar{E}\}\end{Bmatrix}=\begin{Bmatrix}0\\ 0\end{Bmatrix} \tag{A.18}$$

where

$$A_{11}=\bar{m}\omega^2-\left(\frac{AG}{\bar{k}L^2}\right)p^2;A_{21}=-A_{12}=\frac{AG}{L\bar{k}}ip;$$

$$A_{22}=\frac{\bar{m}\omega^2 I}{A}-\frac{AG}{\bar{k}}-\frac{EI}{L^2}p^2$$

The non-trivial solution is achieved by equating the determinant of the coefficient matrix to zero. Then, we have a fourth-order equation with the unknowns, resulting in four values and the displacement functions are obtained as:

$$w(z)=\left[\bar{D}_1e^{ip_1z}+\bar{D}_2e^{ip_2z}+\bar{D}_3e^{ip_3z}+\bar{D}_4e^{ip_4z}\right] \tag{A.19}$$

$$\varphi(z)=\left[\bar{E}_1 e^{ip_1 z}+\bar{E}_2 e^{ip_2 z}+\bar{E}_3 e^{ip_3 z}+\bar{E}_4 e^{ip_4 z}\right] \quad \text{(A.20)}$$

where

$$\bar{E}_n = j_n \bar{D}_n, j_n = \left(-AGip_n / L\bar{k}\right) / \begin{pmatrix} \left(\bar{m}\omega^2 I / A\right) \\ -\left(AG/\bar{k}\right)-\left(EIp_n^2/L^2\right) \end{pmatrix}, (n:1,2,3,4).$$

Finally, the bending moment function $M^T(z)$ and shear force function $Q^T(z)$ of the Timoshenko beam are obtained as:

$$M^T(z)=\left[\frac{EI}{L}\frac{d\varphi}{dz}\right] \quad \text{(A.21)}$$

$$Q^T(z)=\left[\frac{AG}{\bar{k}L}\frac{dw}{dz}-\left(\frac{AG}{\bar{k}}\right)\varphi(z)\right] \quad \text{(A.22)}$$

Using Eqs. (A.19)-(A.22) and Eqs. (17)-(18), the TMM formulations for Timoshenko element frame members can be obtained.